A Study of Mechanisms Governing Single Walled Carbon Nanotube Thin Film Electric Biosensors

by

Andrew Ward

A thesis

presented to the University of Waterloo

in fulfilment of the

thesis requirement for the degree of

Master of Science

in

Chemistry

Waterloo, Ontario, Canada, 2013

Abstract

The successful fabrication and characterization of two chemiresistive platforms for biomolecule detection was demonstrated by this work. The Si/SiO$_2$ based single walled nanotube thin film (SWNTTF) platform was developed to understand the effect of device geometry on pH and M13 bacteriophage sensing capabilities as well as the underlying mechanisms governing SWNTTF chemiresistive biosensors. The dominant mechanism of sensing switched from direct chemical doping to electrostatic gating when the target analyte changed from H$^+$/OH$^-$ ions in pH testing to whole viruses. The experimental limit of detection for M13 for this platform was 0.5pM and an increased sensitivity as well as variability was observed in devices with smaller channel widths. Preliminary device calibration was completed in order to correlate a resistance response to a bulk M13 concentration. The polyethylene terephthalate (PET) based SWNTTF platform was developed to demonstrate the commercial potential of SWNTTF chemiresistive biosensors by detecting relevant concentrations of brain natriuretic peptide (BNP) on economically viable substrates. The pH response of these chemiresistors confirmed that chemical doping was the cause for resistance change in the SWNTTFs. The preliminary results demonstrated successful BNP detection at 50pg/mL using both aptamers and antibodies as recognition elements. Using SWNTTFs as the transducing element of chemiresistors allowed for further understanding of electrical mechanisms of sensing as well as achieving sensitive, real-time and reproducible electrical virus and biomolecule detection. Although these platforms do not achieve ultrasensitive limits of detection, they demonstrate the commercial potential of platforms using SWNTTFs as the transducing element of electrical biomolecule sensors.

Acknowledgements

First and foremost, I would like to thank my supervisor Dr. Shirley Tang. With her support, I was able to further my work in graduate studies. The knowledge and experience I have gained through hands on work in her lab as well as in one-on-one meetings will prove to be very valuable to me in future experiences. My time in her lab as a Masters level student is greatly appreciated. I would also like to thank my committee members Dr. Vivek Maheshwari and Dr. Juewen Liu. I greatly appreciate them taking the time to work with me on my thesis and attend all necessary milestones, especially knowing how busy their schedules are.

I would like to thank Tyler Davidson-Hall for the work he has done involving the cost-efficient biosensors discussed in *chapter 3*. On top of many brainstorm sessions and work with his co-op project, Tyler helped with numerous aspects that are associated with the life of a graduate student. I would also like to thank Anton van der Ven and Anthony Petrie for their all of their advice and help regarding the biomaterials used for testing in this work. Their work ranged from general information and storage to hands on work with culturing bacteria for experiments and it was greatly appreciated.

I would also like to thank all of the members of the QNC Clean Room team including Vito Logiudice, Nathan Nelson-Fitzpatrick, Rodello Salandanan and Brian Goddard. Their continued help and guidance regarding clean room practices and techniques was invaluable to the completion of this project. I would also like to give a special thanks to Nathan for the time he spent with me troubleshooting my project both hands on and in meetings. His help was a big reason for the success of this project. I would also like to thank Hiruy Haile in the science

student machine shop for his time and help with everything involved in the machining of my device prototypes. His help with design and hands on work on my project helped me to realize a final working prototype.

Finally, I would like to thank all other past and present members of the Tang Nanotechnology lab including Louis Cheung, Mike Coleman, David Donkor, Xiguang (Steve) Gao, Zhi Li, Himadri Mandal, Mahyar Mazloumi, Yverick Rangom and Samaneh Shadmehr.

Contents

List of Figures

List of Tables

List of Abbreviations

AFM – Atomic Force Microscope

BNP – Brain Natriuretic Peptide

CVD – Chemical Vapour Deposition

CNT – Carbon Nanotube

CNTTF – Carbon Nanotube Thin Film

DI H_2O – De-ionized Water

DNA – Deoxyribonucleic Acid

DOS – Density of States

EIA – Electrophoretic Immunoassay

ELISA – Enzyme Linked Immunosorbent Assay

fM – Femtomolar

HF – Hydrofluoric Acid

HMDS – Hexametheydisilizane

HRTEM – High Resolution Transmission Electron Microscopy

I_{on}/I_{off} – On/Off Ratio

ISFET – Ion Selective Field Effect Transistor

MIGS – Metal Induced Gap States

MOSFET – Metal-Oxide-Semiconductor Field Effect Transistor

nM – Nanomolar

NSB – Non-specific Binding

PBS – Phosphate Buffered Saline

PDMS – Polydimethylsiloxane

PET – Polyethylene Terephthalate

PMMA – Poly(Methyl Methacrylate)

RBM – Radial Breathing Mode

SB – Schottky Barrier

SCCM – Standard Cubic Centimeters per Minute

SEM – Scanning Electron Microscope

SiO_2 – Silicon Dioxide

SWNT – Single Walled Carbon Nanotube

SWNTTF – Single Walled Carbon Nanotube Thin Film

UV – Ultraviolet

μM – Micromolar

1. Introduction

1.1 Biosensors

Achieving immediate protein, nucleic acid or pathogen detection and quantification at sub-nanomolar (nM) concentrations are highly sought after in the field of analytical chemistry. With the ability to detect and monitor biomolecules at such low concentrations, early detection of potentially harmful species within an individual's system is possible. Devices capable of this could significantly decrease the turnaround time required for conventional and in turn limit the amount of time harmful pathogens have to reproduce and adapt within an individual's system. Further, certain diseases, it is very important to monitor concentrations of specific proteins within blood so any irregularities can be detected. Essentially, true early detection of specific biomolecules is of utmost importance as it can prevent negative effects from occurring. Current methods used to detect biomolecules include enzyme-linked immunosorbent assay (ELISA) and electrophoretic immunoassay (EIA). These methods require long incubation times, complicated instrumentation, sample enrichment and large sample volumes, all of which have to be performed by trained professionals[1].

The inability of these conventional methods to attain real-time detection of biomolecules is inherent in the protocol required to complete a test. An alternative approach must be taken to achieve early detection. Fabrication and characterization of a platform capable of reliable point-of-care, real-time, sensitive and specific biomolecule sensing is the next logical step towards improving on conventional biomolecule detection techniques. A review of literature shows significant interest in fabricating new virus and biomolecule sensing

platforms with some boasting capabilities of detection in serum or whole blood. To date, the leading techniques that are capable of direct detection of biomolecule capture events include whispering-gallery microlasers[2–4], micro-ring resonators[5,6], silicon nanowire field effect transistors (FETs)[7–9], Polymer nanowires[10,11] and surface plasmon resonance[12–15]. These methods have proven to be extremely sensitive, where some cases have even reported single virus detection. However, the detection equipment, complex data analysis and multiple steps prior to capture event signal generation these optical based techniques require greatly hinders their point-of-care capabilities. This is where electrical biosensors have their greatest advantage.

1.1.1 Electrical Biosensors

Real-time and sensitive electrical detection of molecules was brought closer to realization when the first silicon based ion sensitive field effect transistor (ISFET) was proposed and studied by Bergveld in 1970[16]. Since it was first developed, theoretical studies showed that a limit exists to the overall sensing capabilities of these planar electrical biosensors as the devices could only theoretically achieve micromolar (μM) levels of detection[17]. Although these levels are ideal for some types of molecular sensing (i.e. glucose levels in blood), there are many biomolecules of interest that are functional at much lower concentrations. In light of this non-ideal limit, a considerable amount of research regarding one-dimensional electrical biosensors has emerged over the past decade[18]. With ultrasensitive, specific and lab-on-a-chip capabilities, electrical biosensors arise as the ideal candidate for replacing conventional biomolecule detection methods[19].

In essence, there are two main components of electrical biosensors that must work in conjunction to realize a functional device. The first component, called the receptor, is typically a biomaterial. These include proteins, nucleic acids and enzymes that are specific to a target analyte. This component ensures that the only interactions between the target analyte and the biosensor are recognized as a true detection event. The second component, called the transducer, is an electrically active material that has the ability to sense very small electrochemical perturbations in its environment. The material selected for both of these components are of utmost importance as they dictate device properties such as the sensitivity, selectivity and sensing time. *Figure 1.1* schematically shows the typical set up of a two-terminal single walled carbon nanotube thin film (SWNTTF) based electrical biosensor.
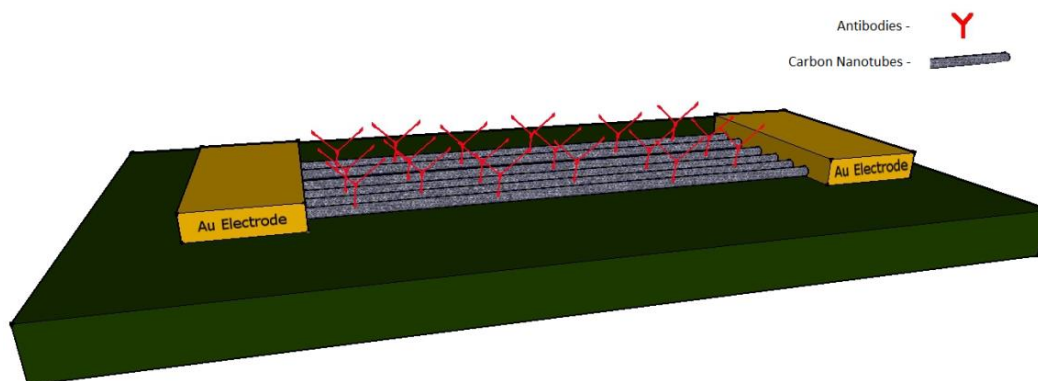
Figure 1.1: Device configuration schematic of an electrical biosensor with a SWNTTF channel coated with antibodies between two gold electrodes. Reprinted with permissions from 20 *copyright 2012.*

The schematic makeup seen in *figure 1.1* truly depicts the simplicity of electrical biosensors. By patterning transducing materials between gold electrodes and subsequently adsorbing receptors onto their surface, sensitive and specific biosensors can be realized. Polymeric and silicon nanowires, which have been used frequently for electrical biosensors, can only be fabricated to as low as 10nm in diameter[21]. This means that they are incapable of

achieving the diffusion properties unique to one dimensional nanomaterials studied by Nair et al[17,22–25]. Using 0.7nm − 2.5nm diameter SWNTs as the transducing component of electrical biosensors, on the other hand, truly takes advantage of these unique one dimensional material diffusion properties[26], which will be discussed anon.

There are a variety of techniques that can be used to fabricate SWNT based biosensors. SWNTs can be grown between the electrodes via catalyst patterning coupled with chemical vapour deposition (CVD), deposited onto a substrate from the solution phase or transferred onto a device following synthesis. Depending on the desired electrical properties of the transducing component, numerous research groups have been able to produce single-SWNT growth between electrodes[27–29] as well as single walled carbon nanotube thin films (SWNTTFs) grown between electrodes[20,30–33]. Some non-growth techniques that are currently used to create SWNTTFs as a channel between electrodes include alternating current electrophoresis while running a SWNT-surfactant solution through a microfluidic channel[34] and SWNT-surfactant solution filtration followed by soft lithography to transfer the SWNTTF into the device[35,36].

Regardless of how the transducer is fabricated, devices are subsequently treated in similar ways in order to make them capable of capturing and sensing a target analyte. Through either physical adsorption or covalent bonds, the receptor molecules are anchored onto the surface of the nanotubes by exposing the SWNTTF to a specific concentration of receptors[37]. There exists a variety of biomolecules that have the ability to selectively attach to a specific analyte due to their unique primary, secondary and tertiary structure. These types of

interactions are seen throughout nature during nucleic acid synthesis where single strand deoxyribonucleic acid (DNA) binds very specifically to its complimentary strand and protein-protein interactions where an antibody recognizes an antigen present in a system. The ability of biomolecules to bind to a target analyte with high specificity is one of the main reasons that there has been such a large push to create electric biosensors.

Engineered nanomaterials that are extremely sensitive to electrochemical changes coupled with specific recognition biomolecules perfected throughout time in nature allow for a truly unique combination of materials. These electric biosensor platforms boast unlimited customizability, which results in these devices possessing a great deal of potential. For example, by using two devices in parallel it is theoretically possible to monitor two different target analytes within the same sample. The receptor component of these two parallel devices can be easily modified prior to testing which allows for multiplex sensing. With this in mind, monitoring multiple target proteins or protein sequences specific to one pathogen or biomolecule is also possible.

To date, SWNT based biosensors have demonstrated ultralow limit of detection levels for a wide variety of analytes. For example, SWNT based platforms boast aM limit of detection for dopamine[38], 25 fM limit of detection for interleukin-6 protein biomarker[39], 100 fM limit of detection for nucleic acid[40] and fM limit of detection for H1N1 influenza virus[36]. In previous work, our group has demonstrated that SWNTTF based electrical devices are capable of 1 pM real-time detection of M13 bacteriophage[20]. These works alone demonstrate the vast capabilities of these electric biosensors. Although there has been an abundance of proof-of-

concept work done in this field, there is still a great deal of debate regarding the mechanistic understanding of electric biosensors[26].

1.2 SWNTs as the Transducing Element

The primary motivation behind using SWNTs as the transducing element of an electric biosensor is their exceptional electrical sensitivity to their immediate environment. This sensitivity is attributed to their unique structure; as all carbon atoms in a molecule are located on the molecule's surface[41]. The high surface area to volume ratio of SWNTs allows all atoms along the SWNT's length to be affected by a variety of surficial interactions, which is optimal for electrical biosensors. Their unique molecular shape also allows for a large surface area available for biomolecule interactions, which enhances the overall sensitivity of the device. As SWNT's are comparable in size to most target analytes and receptor molecules the magnitude of response that occurs as a result of a capture event is significant[42].

SWNTs are the ultimate material for the transducing element of biosensors because of their electronic properties that arise from having a one-dimensional structure[43]. After synthesis, a common way to understand and visualize SWNTs is essentially a rolled up sheet of graphene. This leads to the SWNTs having many electronic properties that are similar to that of graphene in terms of band structure and density of states (DOS). However, energy level quantization is one significant difference that occurs in SWNTs due to boundary conditions that result from their one-dimensional structure[44]. This is the reason individual SWNTs are able to exhibit semiconducting or metallic properties as opposed to graphene. Unless graphene is modified in some way it will always be electrically metallic or a zero-bandgap semiconductor. Depending on

the orientation of the hexagonal building blocks of a SWNT, allowed energy levels determine whether the SWNT is metallic or semiconducting[43]. Researchers to this day are still unable to completely control the chirality of the SWNTs during synthesis. An uncontrolled growth of a SWNT network or forest will yield a 2:1 ratio of semiconducting:metallic SWNTs based on experimental and theoretical studies[45]. Due to the limitations in SWNT synthesis, device design plays a big role in achieving favourable reproducibility and device performance.

In a typical two-terminal setup, the overall conductance of the SWNT is tuned by chemical interactions that occur in proximity to their surface. A sensitive transducing component requires a low DOS around the Fermi level. Having a lower DOS around the Fermi level results in the material being more sensitive to energy changes induced by electrochemical interactions occurring during capture events. This leads to the conclusion that semiconducting SWNTs used as the transducing element are ideal as their lower DOS around the Fermi level meets this requirement[31]. Increases or decreases in energy for these tubes are likely to induce large conductance changes. Metallic SWNTs, on the other hand, do no exhibit these increased sensitivity properties due to the fact their DOS is constant around the Fermi level[43].

There are still many issues involved with fabrication of SWNT based biosensors concerning reproducibility. In terms of CVD based growth of SWNTs, previously mentioned random chirality is the main reason that as grown single-SWNT based sensors have very low reproducibility's. Not only does the SWNT have to bridge an electrode gap during growth, but with a successful growth there is no guarantee of the properties that specific SWNT will exhibit. Solution based techniques used to fabricate SWNT based devices involve coating the nanotubes

with surfactants and subsequently sonicating the solutions for dispersion. These techniques generally hinder the electrical properties of the resultant SWNT thin film. Mechanical cleavage under sonication and surfactant coatings are typically the cause of this[46]. Additional material coating the SWNTs decreases device sensitivity as the nanotubes are not directly exposed to the environment. The main setbacks for SWNT based biosensors are researcher's inability to control the properties of as grown SWNTs as well as damaging and contamination during solution based fabrication.

1.3 SWNT Biosensor Theoretical Background

The first SWNT based transistors were reported in 1998 by the Avouris group from IBM[47] and the Dekker group from Delft University[48]. Since this time, there has been significant progress made towards characterizing various SWNTs properties as well as integrating SWNTs into working devices. Moving forward, numerous research groups worldwide have been concentrating on using these SWNT transistor type devices to sense a variety of chemical and biological species in a proof-of-concept matter. Although many of these works have demonstrated quite exceptional results, there are still a few underlying issues that must be studied and explained with experimentation. Mechanisms governing electrostatic interactions between biological species, SWNTs and device electrodes are not completely understood. This confusion is the underlying reason for disagreement between numerous research groups to date[19,26,33]. Regulation agencies such as Health Canada and the Food and Drug Administration require exhaustive research and characterization of health monitoring devices. Therefore, to approach commercialization for SWNT based devices, there must be a thorough understanding

of the mechanisms governing the detection of biomolecule capture events so that experimental data can be reproduced consistently.

Theories outside of electrostatic interactions have also been proposed to explain why increased sensitivities have been observed for low dimensional devices[17]. It is reported that only a theoretical 5-10 times increase in device sensitivity should occur because of unique low dimensional electrostatic properties of the transducer. However, experimentation has proven that changing the transducer from planar structures to one-dimensional structures sensitivities have increased from µM to femtomolar (fM) levels of detection in some cases. In order to explain such a large increase in sensitivities of these low dimensional devices, the kinetics of diffusion has been thought to play a large role[17]. Further work towards studying the kinetic response of nanobiosensors is required to support this theory.

1.3.1 Proposed Sensing Mechanisms

As aforementioned, there is still a great deal of debate taking place regarding the various sensing mechanisms that dominate the SWNT based biosensor response. To date, there have been five main mechanisms theorized by the scientific community, which all involve electrostatic interactions between the receptor and analyte resulting in an electrical change induced in the SWNTs[26]. These mechanisms include chemical doping[27,49–54], electrostatic gating[55–57], Schottky Barrier (SB) modulation[58–61], capacitive coupling[28,29,31,32,51,62–64] and carrier mobility changes[65,66]. All of these mechanisms involve probing the electrochemical interactions between the target analyte and the anchored receptor molecules. Each mechanism affects the SWNT's electrical properties in its own unique way. In order to fully understand this problem, a

detailed description of all sensing mechanisms is required. *Figure 1.2* shows the results of a

simulation regarding the effect that all four types of sensing mechanisms.
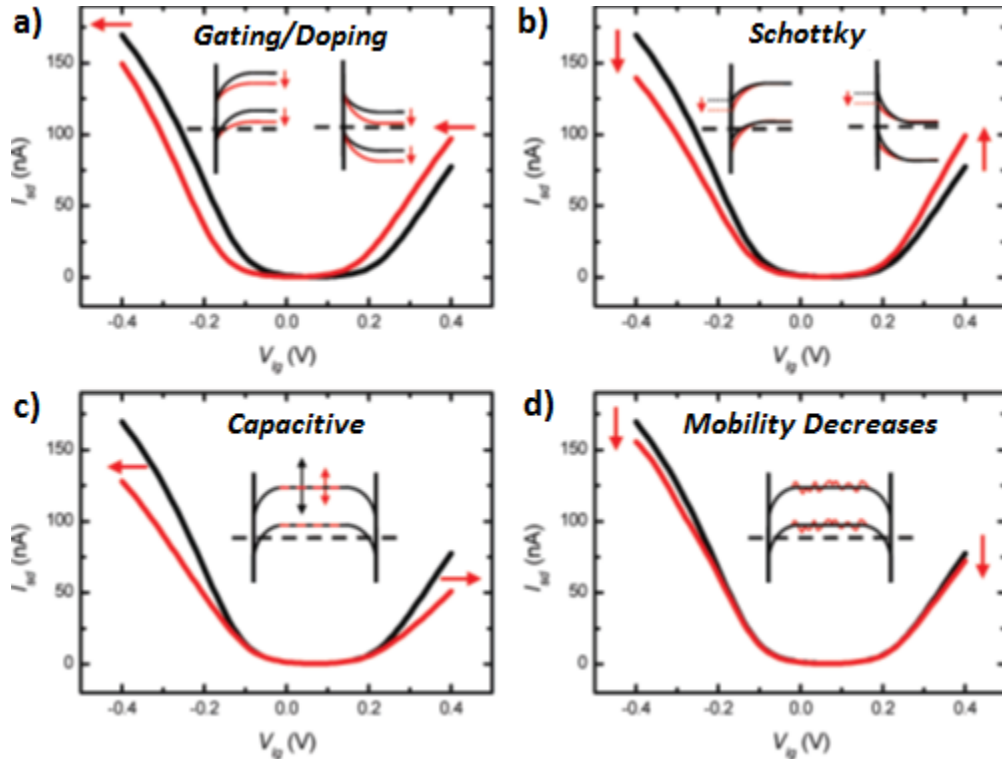
Figure 1.2: Simulated I_d-V_g curves for before (black) and after (red) protein adsorption for the (a) Electrostatic gating/chemical doping mechanisms, (b) Schottky barrier modulations, (c) Capacitance Coupling, and (d) Mobility Carrier Changes. Insets depict changes to the SWNT's band structure. Reprinted with permissions from 26 copyright 2008.

Figure 1.2 demonstrates that there are subtle differences in the way that each proposed

sensing mechanism affects the CNT channel's electrical properties. The study goes into detail

regarding how these interactions affect both the characteristic I_d-V_g curve as well as the

electronic band structure of SWNT devices. It also gives insight into how one would be able to

isolate a single type of sensing during experimentation in order to study them individually.

1.3.1.1 Electrostatic Gating

Electrostatic gating is a very important theory that occurs because all biomolecules are capable of carrying a net charge. The net charge of a biomolecule depends on its primary structure (sequence of its amino acids, nucleotides, etc.) as well as solution conditions (pH, ion type, ion concentration, etc.)[67]. Specific to physiological conditions, it is highly probable that a biomolecule will have a net charge or at least a number of regions with charged groups that are all at the surface of the protein. Protein folding occurs so that its polar regions act to shield the hydrophobic sequences from water in order to minimize the systems free energy. As a protein containing charged regions adsorbs onto or near the surface of the SWNT, the biomolecule will induce an electrostatic gating effect on the SWNT[57].

It is also likely that adsorption of biomolecules can act to trap ions on the substrate of the devices. This results in a gating effect that is a consequence of an altered electric field around the SWNTs, thereby tuning the carrier density in the channel by shifting the Fermi energy. This mechanism effectively shifts the threshold voltage of the device resulting in a polarity dependent change in film conductance. This effect can be seen in the shift of the threshold voltage in the I_d-V_g curve in *figure 1.2(a)*. It is of note that this mechanism does not change the subthreshold swing or the on/off drain currents of the device.

One factor that must always be taken into consideration regarding this theory is the ionic strength of test solution. This is because the ionic strength of the solution surrounding the transducing material has a large effect on the SWNT's Debye length. The Debye length is a measure of the distance into the surrounding solution a surface is able to experience

electrostatic changes[68]. This occurs in solution due to the double layer of charged ions that build up on the surface so that electroneutrality is maintained. Typically, OH$^-$ and H$^+$ ions in aqueous conditions are charge-determining ions for most surfaces, especially in dilute buffer conditions[69]. The double layer acts to screen out any electrostatic effects that occur any distance further than the Debye length away from a surface. *Equation 1* shows the formula used to calculate the Debye length in solution:

$$\delta = \sqrt{\frac{\varepsilon_o \varepsilon_r K_B T}{2 N_A e^2 I}} \qquad (1)$$

Where δ is the Debye length, ε_o is the relative permittivity of the solution, ε_r is the permittivity in vacuum, K_B is Boltzmann's constant, T is the temperature (in Kelvin), N_A is Avogadro's Number, e is the elementary charge and I is the ionic strength of the solution (in mole/m^3)[68]. The Debye length within the solution is inversely proportional to the ionic strength of the solution. This is understandable as the electrolyte solution screens more effectively if there are more ions within the solution. This demonstrates that low concentrations of ions in solution yield optimal conditions for sensing biomolecules via electrostatic gating. A Debye length that is on the order of the size of a receptor biomolecule (~10 nm) allows for the transducing material to sense the effects of electrostatic interactions during capture events[68].

1.3.1.2 Chemical Doping

Chemical doping is a mechanism of electrical detection that involves the direct transfer of electrons from charged species to and from the SWNTs[26]. This mechanism of sensing is responsible for the SWNTs electrical response to a variety of gases and liquids. Essentially, any

adsorbed species on the surface of the SWNT is capable of donating or taking away some fraction of an electron in order to tune the overall conductance of the nanotube[70]. This mechanism requires direct contact between the nanotube and the charged species.

Figure 1.2(a) shows the effect that an electron donor would have on a p-type semiconducting SWNT. The threshold voltage of the SWNT would be shifted in the negative direction as the hole population depletes. It has been proven that rather than the conductance of the nanotube being affected by the overall charge of the dopant molecule, the redox state of the molecule is what dictates the direction of conductance change[49].

1.3.1.3 Schottky Barrier Modulation

The second mechanism that is of importance to SWNT based biosensors deals with modulations to the SB that exists at metal-semiconductor interfaces. The SB occurs in these devices due to the fact that when two materials come together and are at equilibrium, the Fermi level at the bulk of both materials must be equal. However, due to the interfacial interactions, there is a finite DOS within the bandgap of the semiconductor know as metal induced gap states (MIGS) which are all occupied below the Fermi level[71]. The exponential decrease of these states towards the bulk of the semiconductor creates a dipole that results in the formation of a SB. This creates a barrier felt by the charge carriers when they arrive at a metal-semiconductor junction. These interfacial properties in effect "pin" the Fermi level in the middle of the bandgap at the interface and ensures that the charge carriers always encounter the barrier.

In SWNTs, however, Fermi level pinning is circumvented due to their one-dimensional geometric nature. This results in localizing the dipole in all three directions, which in turn decreases the SB width to approximately 2 nm in comparison to infinite distances for a planar interface[72]. With this in mind, the choice of the metal electrode plays a large role as its work function essentially tunes the p- or n-type behaviour of the SWNT channel. In terms of sensing experiments, the mechanisms behind SB modulation involve passivating the SWNT channel and tuning the metal electrode work function as biomolecules adsorb onto the electrode surface[73]. This results in changes to the size of the SB that charge carriers are subject to within the device and in turn modulates the device's conductance properties. This effect can be seen in *figure 1.2(b),* where the SB modulations occurring within the device changes the overall subthreshold swing as well as the on current of the nanotube.

Aside from the contact metal-semiconducting nanotube junctions, there are a variety of junctions that arise within SWNTTFs. The electronic properties of an individual nanotube within a SWNTTF is random as CVD growth techniques used in this work follow a 2:1 ratio of semiconducting to metallic nanotube distribution[74]. This results in a myriad of junctions within a single SWNTTF capable of modifying the film's electronic properties. Therefore, understanding Schottky barrier modulations and their overall effect on SWNTTF conductance is imperative to improving biosensor sensitivity and reproducibility.

1.3.1.4 Capacitive Coupling

This mechanism involves modifications to the relative permittivity of the double layer as well as the resultant electric field around the SWNT[57]. The total capacitance of the SWNT

channel is dependent on a series addition of a built in and external capacitances depicted in *Equation 2*[28]:

$$\frac{1}{C_{Total}} = \frac{1}{C_{DL}} + \frac{1}{C_q} \tag{2}$$

Where C_{Total} is the capacitance per unit length of the SWNT, C_q is the quantum capacitance of the SWNT and C_{DL} is the electrochemical double layer capacitance at the SWNT-liquid interface. In essence, the quantum capacitance is a unique property of SWNTs which occurs due to the charge of the electric double layer as well as the SWNTs finite DOS[75]. This overall capacitance is important as *Equation 3* shows that its value is directly proportional to the overall conductance of the channel in the diffusive regime where conductance is still sensitive to the gate voltage[28]:

$$G = \frac{C_{Total}|U_{lg} - U_{go}|\mu}{L} \tag{3}$$

G is the conductance of the SWNT channel, C_T is the total capacitance, U_{lg} is the liquid-gate voltage, U_{go} is the threshold voltage of the device, μ is the mobility of the charge carriers and L is the length of the channel. Typically, $C_q \ll C_{DL}$ due to the finite DOS within the SWNT limiting the amount of charge able to build up on the SWNT, meaning that most of the time the C_q will dominate the total capacitance[28,63]. During sensing experiments, the ions built up in the double layer are replaced by larger biomolecules with different relative permittivity's resulting in a change in the C_{DL}. At specific amounts of surface coverage with biomolecules with dissimilar permittivities, the C_{DL} can be small enough to affect C_T. *Figure 1.2(c)* shows that this

sensing mechanism results in changes to the subthreshold swing of the device as the C_T only tunes *Equation 3* in the subthreshold region.

1.3.1.5 Carrier Mobility Decrease

The final sensing mechanism that has been proposed involves charge carriers having their mobility decreased within the SWNT channel. The main principle behind this theory is that analytes adsorbed on the surface of the SWNTs act as scattering sites which result in lowering the carrier mobility within the SWNT[65]. This method of sensing typically involves chemical functionalization of the SWNTs which act as scattering sites as they are seen as defects in their highly crystalline structure. Typically, when the SWNTs have not been chemically functionalized and instead have molecules adsorbed onto their surface, they do not exhibit this type of sensing[26]. *Figure 1.2(d)* shows that this mechanism induces small changes in the subthreshold swing but mainly decreases the overall on state current when more scattering occurs in the SWNT.

1.3.2 Diffusion Capture Theory

Nanostructures as transducing components in electrical biosensors have shown an increase of over 6 orders of magnitude compared to their planar counterparts (i.e. silicon nanowires versus planar silicon)[17]. However, all electrostatic considerations are only able to explain a 5-10 times increase in the sensitivity. Further explanation is required in order to understand and exploit the greater sensitivity observed in lower dimensional devices. It was recently theorized that nanobiosensors show such increased sensitivities due to the fact that their low dimensional structure (approaching 1-2.5 nm in diameter for SWNTs) have the

majority of their structure exposed to the environment. This can be understood easily by comparing a SWNT to planar silicon as all carbon atoms are at the surface of a SWNT while many silicon atoms reside away from the planar silicon's surface. The increased surface area to volume ratio is likely to play a large role in determining the overall sensitivity of a device. Theoretical simulations have shown that the diffusion of biomolecules have a large dependence on the geometry of the transducing material, which in turn dictates the device's sensitivity and response time[17].

The diffusion-capture theory states that there exists a limit to the concentration of biomolecules that can be detected due to diffusive transport. To understand this theory, the capture capabilities of a biosensor must be analyzed through *Equation 4*[17]:

$$\frac{dN}{dt} = k_f(N_o - N)\rho_s - k_R N \qquad (4)$$

Where N is the density of conjugated receptors, N_o is the density of receptors on the sensor surface, k_f and k_R are the capture and dissociation constants, and ρ_s is the concentration of analyte particles at the sensor surface at any given time. In a system using biomolecules (such as deoxyribonucleic acid (DNA) or antibodies) with high k_f/k_R ratios the latter term in *Equation 4* is approximately 0[76]. The next step is to incorporate diffusion mechanisms through *Equation 5*[17]:

$$\frac{d\rho_s}{dt} = D\nabla^2 \rho_s \qquad (5)$$

Where D is the diffusion constant of the target analyte in solution. By taking the integrated flux into account and incorporating the diffusion-capture models, this group was

able to find that the time dependent number of particles at the sensor surface can be monitored using *Equation 6*[17]:

$$N(t) = \rho_o t \left(\frac{A_D}{C_D(t)} + \frac{1}{k_f N_o} \right) \qquad (6)$$

Where ρ_o is the concentration of target analyte at the bulk-depletion region interface, A_D is the surface area of the biosensor and $C_D(t)$ is the diffusion capacitance which depends on the dimensionality of the sensor. At some point in time, the number of captured analyte results in a detectible signal in the SWNT transducer, known as N_s.

In order to understand diffusion capacitance, one has to imagine there are two parallel plates existing in these electrical biosensor systems. The first plate is the surface of the sensor and the second plate is the interface at which the bulk concentration exists. This property of electronic biosensors sparked the idea that a diffusion capacitance exists in these systems. The diffusion capacitance is analogous to regular capacitance for parallel plate capacitors, where the dielectric constant is replaced by the target analyte's diffusion constant. As there are different dimension transducing components, each has its own diffusion capacitance, which can be seen in *Equations 7 and 8*[17]:

$$\text{Planar:} \qquad C_D(t) = \frac{D}{\sqrt{2Dt}} \qquad (7)$$

$$\text{One-Dimensional:} \qquad C_D(t) = \frac{2\pi D}{\log\left[\frac{\sqrt{4Dt} + a_o}{a_o}\right]} \qquad (8)$$

Where a_o is the radius of the one-dimensional channel in the biosensor. There is a fundamental difference between the time dependence of the diffusion capacitance of the

planar system and the one-dimensional system. In the planar system, there is a $t^{-\frac{1}{2}}$ dependence whereas in a one-dimensional system there is a much more complicated time dependence. This plays a large role in the kinetic response of the two different systems as the time required for a target analyte to diffuse to the surface varies depending on the device dimensionality. *Figure 1.3* contains a schematic that will help to understand why there is a difference in the time dependence for these two systems.

a) $W=(2Dt)^{1/2}$ **b)** $W=(4Dt)^{1/2}$
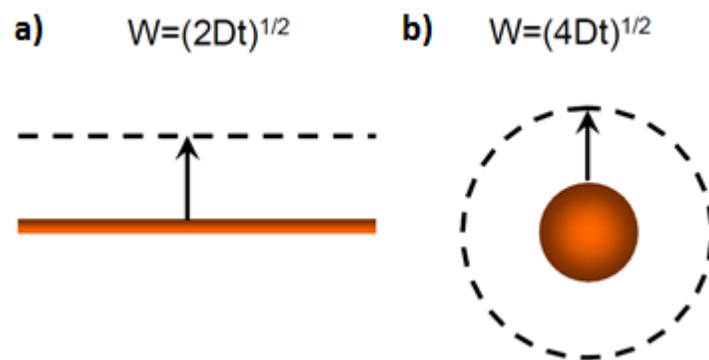
Figure 1.3: Schematic showing the time dependence of distance (W) at which equilibrium concentration (ρ_o) is from the surface of the receptor for (a) a flat brown two-dimensional planar device and (b) a cylindrical brown one-dimensional Nanowire. Reprinted with permissions from 17 *copyright 2006.*

Figure 1.3 demonstrates that in both systems, the distance at which equilibrium is achieved in solution moves further from the sensor surface as time progresses. Over time the regions that are closest to the sensor's surface are depleted of the target analyte as a result of capture events occurring. For the planar system, as time proceeds the bulk concentration moves further from the surface resulting in diffusion limiting the amount of analyte molecules that are able to reach the sensor's surface. However, for the one-dimensional system, even though the bulk concentration is also moving further from the surface with time, an increase in W results in the surface area of the target analyte concentration plane also increasing. This essentially results in reducing the effects of a larger diffusion distance that analyte molecules

must travel in order to be captured by the sensor. A simulation highlighting the difference in sensitivity due to diffusion kinetics for one-, two- and three-dimensional transducing elements can be seen in *figure 1.4*.
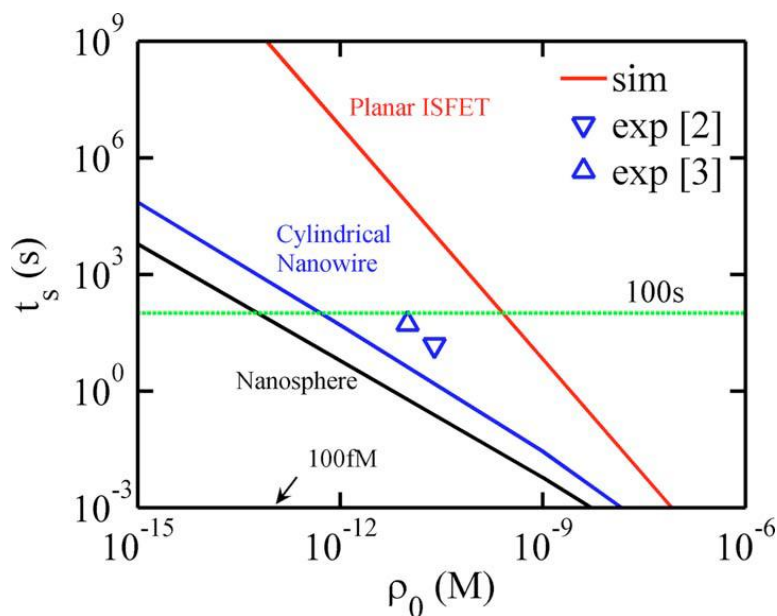
Figure 1.4: Diffusion-capture theory simulation of settling time vs. bulk analyte concentration between planar (red), one-dimensional (blue) and zero-dimensional (black) biosensors. Blue triangles indicate reported results for one-dimensional sensors. Reprinted with permissions from 17 copyright 2006.

Figure 1.4 effectively shows the difference between the detectible limits of planar and low dimensional biosensors based on the diffusion-capture theory simulations. The theory is able to explain and predict sensitivity limits between the different biosensor systems; the simulations show that there is room for improvement for reported one-dimensional biosensors as well as a requirement for additional experimentation to confirm these findings.

The theoretical study and simulation reported considered smaller biomolecules such as proteins or nucleic acids as the target analytes. When studying whole viruses rather than small molecules, there are a few major differences in the properties that must be kept in mind. The

first of these properties is the size difference between small molecules (i.e. DNA, Proteins, etc.) and viruses. As it is known that the diffusion coefficient is inversely proportional to molecular weight, larger species such as viruses have smaller diffusion coefficients[77]. This will result in a decrease in the diffusion capacitance of the one-dimensional system. However, this is not expected to hinder the device's sensitivity as a single virus particle is in theory able to have multiple capture events occurring with the sensor resulting in an increase in the signal.

2. Silicon Based SWNTTF Biosensors

2.1 M13 Bacteriophage Biosensors

The M13 bacteriophage is a filamentous virus that infects particular strains of Escherichia Coli (E. Coli) carrying the F plasmid[78,79]. This virus consists of a single stranded loop of DNA that is enclosed in an approximately 1μm long tube-like array of 2700 coat proteins[80]. The pIII coat protein, which is the phage's largest and most complex coat protein, is necessary for host recognition and cell infection[81]. Previous studies have shown that electrical biosensors using SWNTTFs coupled with anti-pIII M13 antibodies are able to selectively detect 1pM concentrations of whole M13 bacteriophage only when the pIII coat protein is present[20]. The tube like structure and size of the phage as well as the proof-of-concept work previously done in this lab made M13 an attractive candidate for a systematic study of SWNTTF chemiresistive biosensors.

To facilitate the shift of our SWNTTF based biosensors from proof-of-concept to commercialization, research must advance toward studying the underlying mechanisms of electrical sensing. Full characterization of the interactions between the analyte, receptor and transducer must be completely understood in order for reproducible and reliable pathogen detection and quantification to be achieved. Direct comparison of numerous parallel SWNTTFs in pH controlled environments prior to pathogen detection can help to understand some of the mechanisms at play in these devices. In addition to SWNTTF density optimization that has been studied[32], film geometry is a design consideration that can be used to further optimize reproducibility and sensitivity SWNTTF containing devices.

2.2 Fabrication and Methods

2.2.4 Prototype Design and Fabrication

The aim of this project was to fabricate 32 SWNTTF devices of ranging geometries in parallel on a Si/SiO$_2$ substrate. Then, using a microfluidic channel along with a device mount a prototype capable of monitoring electrochemical changes and sub-nanomolar concentrations of virus in solution was fabricated. All information pertaining to the synthesis of the SWNTTFs, substrate fabrication, device cleaning, microfluidic channel fabrication and sample delivery can be found in *appendix A*. The prototype design involved a number of iterations as well as trial and error in order to obtain reliable fluid flow and electrical connections. The final prototype and schematics pertaining to its design and operation can be found in *figure 2.1*.
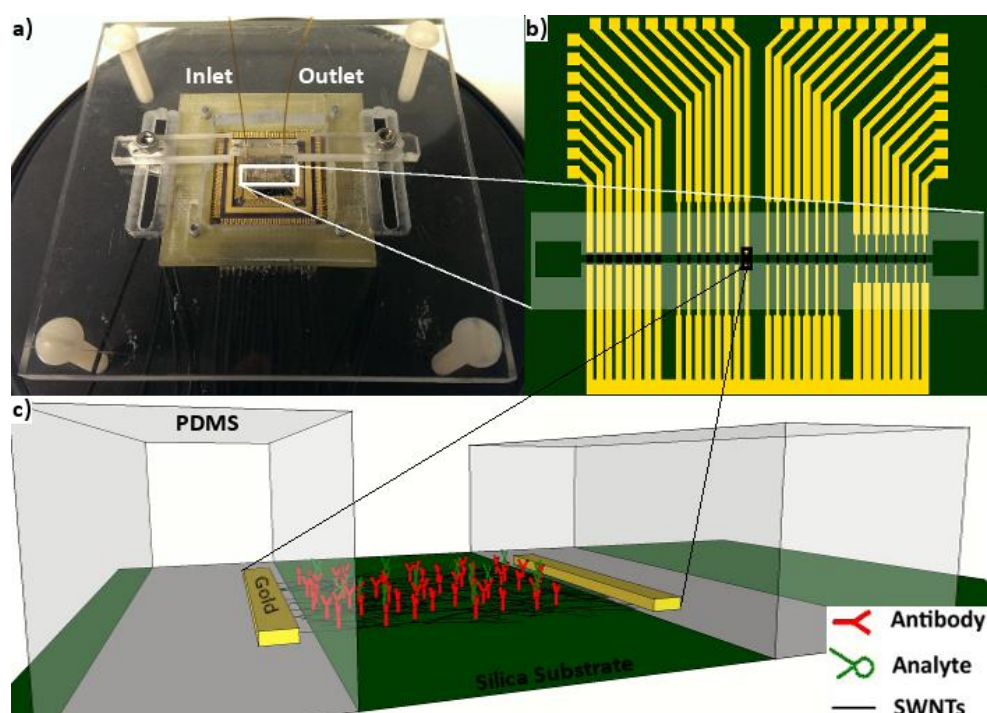
Figure 2.1: Images of (a) Prototype with device wire bonded to a chip holder mounted to a Plexiglas base. A PDMS microfluidic channel is clamped down to the surface of the chip, (b) the silica substrate with patterned electrodes, SWNTTF and PDMS channel and (c) single device showing antibodies capturing target analytes on the surface of the SWNTTF.

Figure 2.1(a) is an optical image of the final prototype used in this study. The main features of the prototype include a Plexiglas base, chip holder, custom made socket, PDMS microfluidic slab, fused silica tubing (Polymicro Inc.) and the Si/SiO$_2$ substrate with SWNTTFs. In order to electrically probe the SWNTTFs during characterization and sensing experiments, a very simple two-terminal gold electrode setup, shown in *figure 2.1(b),* is employed. *Figure 2.1(c)* is a schematic depicting a SWNTTF based electric biosensor during a sensing experiment.

It is important to note that the dimensions of the microfluidic channel only expose approximately 100μm of each SWNTTF and the SiO$_2$ substrate beneath it. The setup for this device includes 32 electrode pairs that are electrically connected with the patterned SWNTTFs bridging them. Four different film dimensions are used in this study including eight films at 150μm x 100μm, 150μm x 50μm, 150μm x 25μm and 150μm x 10μm. Some sensing mechanisms mentioned in *section 1.3* are theoretically dependent on the SWNTTF dimension. This is why all films were designed to be in parallel during testing for direct comparison in identical conditions. A common ground is used in this setup in order to further simplify probing during experimentation.

Conventional systems using SWNTs for sensing biomolecules include a liquid gate so that I$_d$-V$_g$ measurements can be used to determine the switching capabilities of the devices. However, the gate electrode is exposed directly to the test solutions and some groups have observed that based on electrode composition it can actually be responsible for the response seen from these devices rather than the SWNTs[82]. Aside from maintaining a very simple setup

for testing, removing the gate electrode will ensure that external contributors to signal change do not exist.

2.2.5 Dry State Characterization

Dry state material characterization of all devices is vital and must be completed throughout fabrication. Raman spectroscopy is the simplest method of determining whether or not SWNTTF synthesis is successful prior to film transfer. Raman peak analysis after transfer and patterning can then be used to ensure that no damage has come to the SWNTs during fabrication, especially important for fabrication steps involving plasma etching. All Raman spectra were measured using the Horiba (Jobin Yvon) HR800 Raman spectrometer.

Imaging techniques such as atomic force microscopy (AFM) and scanning electron microscopy (SEM) are used to determine the density of the SWNTTFs after synthesis. Since the aim of this project is to use low density films that have an enhanced sensitivity to biomolecules, this characterization is very important. Ensuring that the synthesis techniques used in this study are indeed capable of producing such low density films was the first goal of this project. In addition to establishing synthesis parameters that result in an ideal density, these imaging techniques are used to determine whether device patterning and cleaning protocols were completed successfully during device fabrication. Nanotube properties prior to biomolecule detection such as tube diameter and tube junction height can be measured using the AFM section analysis tool. All AFM imaging was completed using Digital Instruments Nanoscope Multimode AFM.

One of the primary aims of this project is to determine whether a correlation exists between the dry state electrical behaviour of the SWNTTFs and their electrical response to biomolecules. This means that dry state electrical characterization is required to complete this study. The devices are fabricated in a way such that back-gating through the 50nm SiO_2 is possible. Using a gate voltage varying from -5V to 5V the drain current was monitored at a constant drain voltage of 10mV. With this information, an on/off ratio (I_{on}/I_{off}) can be determined in order to establish the overall switching capability of the film, which in turn can be compared to the device response during biomolecule sensing experiments. The dry state resistance of each device is also determined. With a drain voltage varying from -0.5V to 0.5V, the drain current of each device is measured. All electrical measurements were performed using the Agilent B1500A Semiconductor Analyzer.

2.3 Results and Discussion

2.3.1 Dry State Characterization

Device fabrication requires characterization at every stage to ensure all protocols are working properly. The simplest way to ensure pristine nanotubes are present in the SWNTTF is to measure the film's Raman spectrum. *Figure 2.2* shows a typical SWNTTF using the aforementioned synthesis recipe at a number of stages during fabrication.
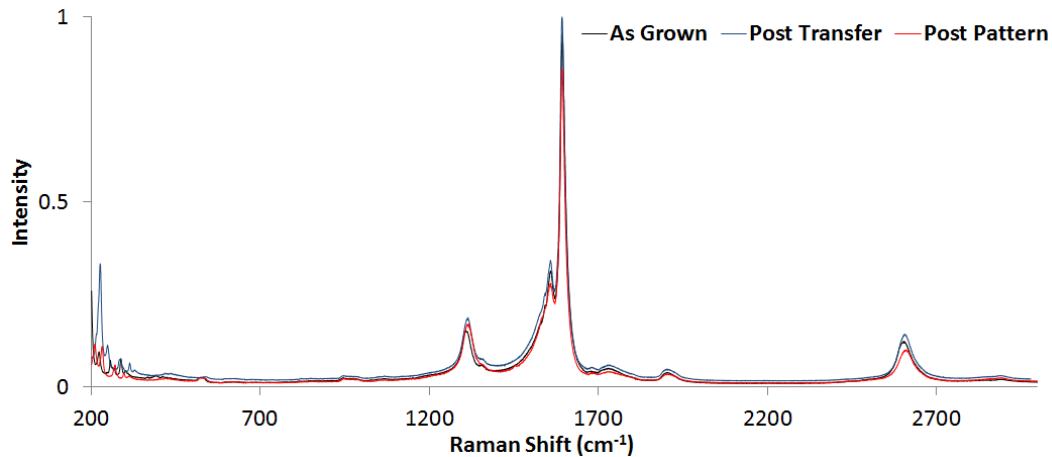
Figure 2.2: Raman Spectra of a SWNTTF taken post growth, post transfer and post patterning.

The first important conclusion that can be made after analyzing *figure 2.2* is the fact that the SWNT synthesis performed is indeed successful. It is also clear that all fabrication steps did not damage the SWNTs. This synthesis technique results in a random and uncontrolled growth of SWNTs as the silica nanoparticles are loaded with a cocktail of catalyst metals. This means that along with a random placement of catalyst on the substrate during spin coating there is also no control over the individual radius or electrical nature of a SWNT, or the SWNTTF as a whole. The result of this growth is a statistical average of approximately 33% metallic and 66% semiconducting nanotubes randomly oriented as a network of carbon nanotubes. The location, number and intensity of peaks within the radial breathing mode (RBM) range[83], between $120cm^{-1}$ to $250cm^{-1}$, are consequently random for a given spot on the SWNTTF. With this considered, all samples measured do contain a number of RBM peaks with a rich underlying signal in the region indicating that the carbon nanotubes are indeed single walled. Other peaks of importance that indicate the films are composed of SWNTs are the D, G and 2D bands located at approximately $1350cm^{-1}$, $1600cm^{-1}$ and $2700cm^{-1}$, respectively. It is worth noting that

the majority of samples show a very high G:D band ratio (on average 8-10) indicating that the film contains pristine SWNTs.

By comparing the three stages of fabrication shown in *figure 2.2*, it is clear to see that every step in the fabrication of the final device does not damage or harm the SWNTs in the film. This is concluded due to the fact that the Raman peaks pertaining to SWNTs in each spectrum are preserved throughout fabrication. All changes in intensities can be attributed to the fact that some steps involve coating the SWNTTF in photoresist which has been seen to supress some peaks (mainly RBM peaks). Further, a change in the laser spot location is likely to shift the peak intensities as well.

After determining that successful growth, transfer, patterning and cleaning occurred, the density of the SWNTTFs were determined. AFM measurements as well as section height analysis of a SWNTTF obtained using this synthesis protocol can be seen in *figure 2.3*.
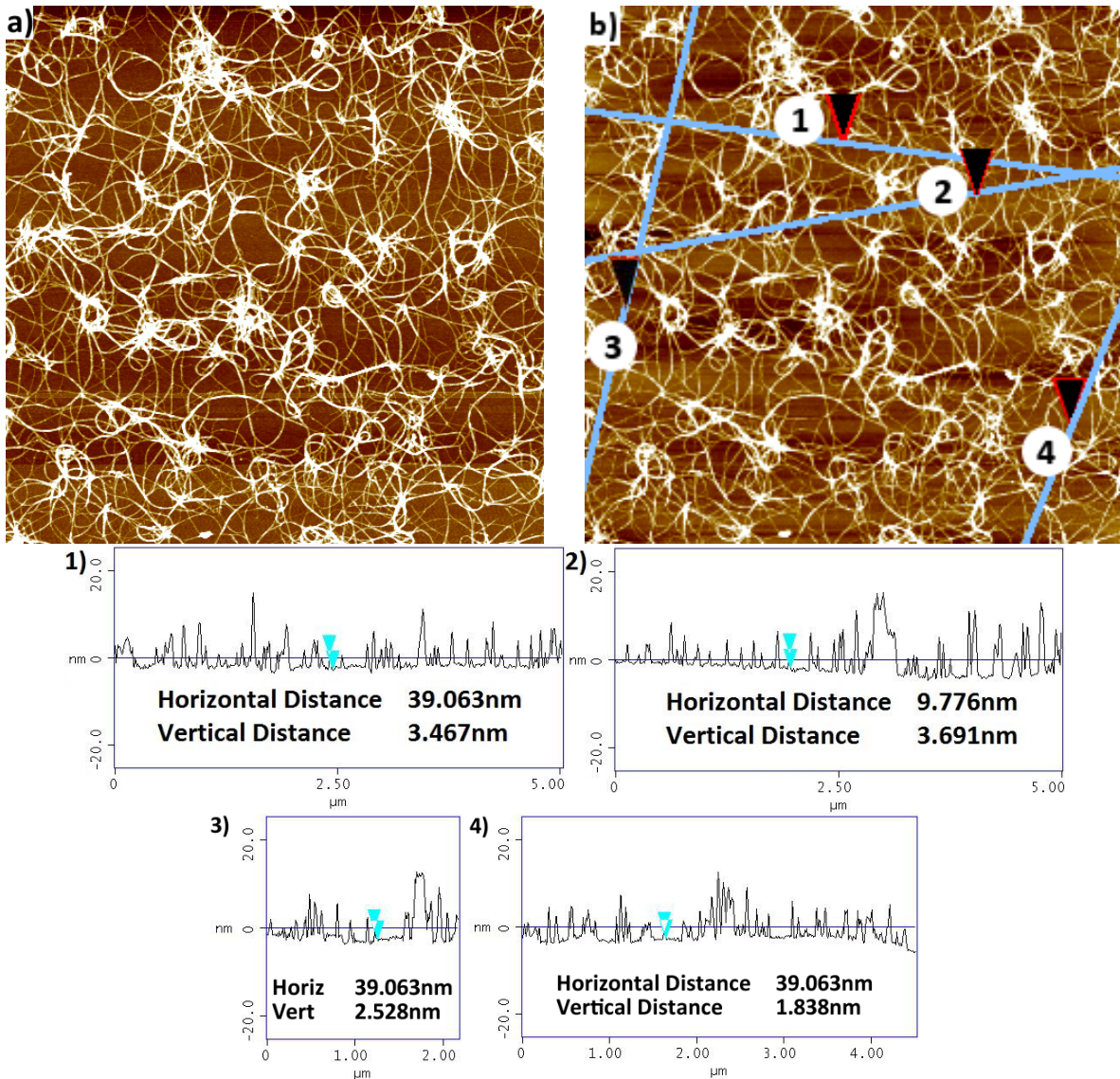
Figure 2.3: AFM characterization of SWNTTF including (a) the original image of the low density SWNTTF, (b) the AFM image indicating the location of height measurements along the image section (blue lines) and (1-4) the height measurements along each section.

Figure 2.3(a) shows an AFM image of the typical sub-monolayer SWNTTF synthesized using the aforementioned synthesis protocol. Nanotube bundling is evident in this image and is a consequence of randomly placing catalyst loaded nanoparticles on the substrate via spin coating. Recent studies have shown that lower density SWNTTFs are capable of achieving higher sensitivities for biomolecule detection[32]. According to percolation theory as well as experimental and simulation work, lower density films are more dependent on semiconducting

tubes[74,84], which are in turn more sensitive to energy shifts around the Fermi level[43]. In light of this, our devices were modeled after these films in order to exploit the enhanced sensitivity that can be achieved by using low density films. In addition to film density measurement, it is also important to use AFM imaging to confirm some of the conclusions made with Raman spectroscopy regarding the nature of the nanotubes.

A number of sections containing seemingly isolated nanotubes were chosen for AFM section and height analysis, which can be found in *figure 2.3(b)*. The blue lines indicate the section chosen for analysis while the numbered arrows indicate the exact spots chosen for direct height measurement. *Figures 2.3(1)-(4)* show the height profile, blue lines with arrows indicating measurement locations and finally the horizontal and vertical measurements. *Figure 2.3(4)* demonstrates that the film does indeed contain SWNTs diameter measured was 1.8nm. Other measured areas showed larger radius measurements for single nanotubes, with measured diameters ranging from 2.5nm-3.6nm. As these latter measurements are on the higher end for SWNT radii, with some areas having even larger measurements, it is highly probable that bundling of nanotubes into ropes occurs during synthesis[85]. It was also observed that along the section there are a number of tubes that show a very similar height profile along with large height variations at areas where bundling or stacking occur of tubes occurs. These observations, along with the curvature the nanotubes possess[85], are indicative of the carbon nanotubes in these films being single walled. Double walled nanotubes existing within the film is also possible, however, previous studies using high resolution transmission electron microscopy (HRTEM) have shown that the majority of the film is indeed single walled tubes[86].

The final dry state characterization involves determining the switching capabilities of the semiconducting tubes in the SWNTTF. The I_{on}/I_{off} as well as the average switching capabilities of the films can be seen in *figure 2.4.*
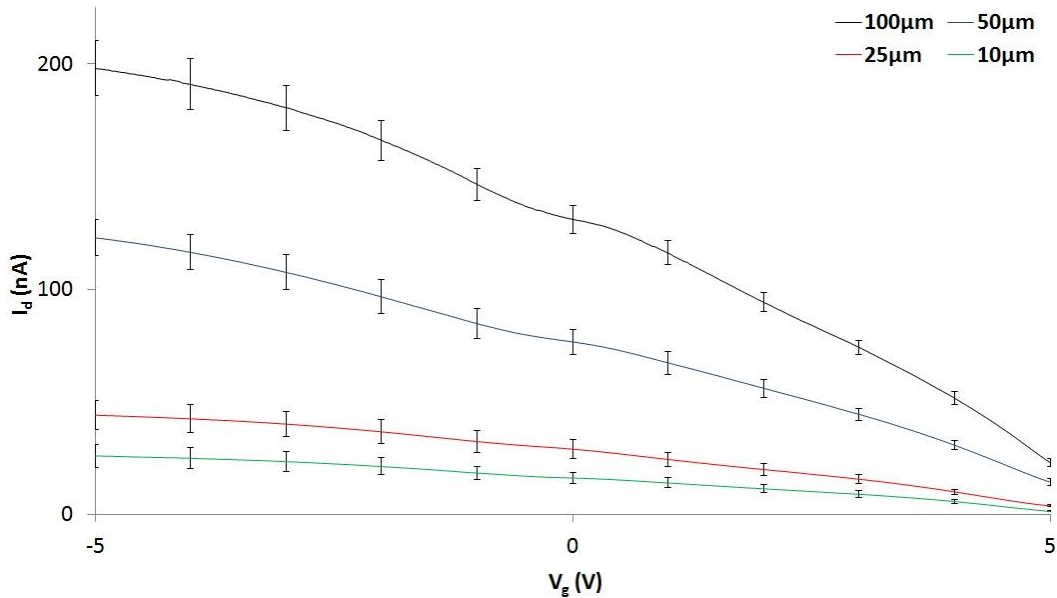
Figure 2.4: Average I_d-V_g characteristic curves for all dimensions of the SWNTTFs used in this study.

Figure 2.4 shows the average I_d-V_g characteristic curves of the SWNTTFs for all channel widths. Decreasing drain current with respect to an increasing gate voltage is indicative of a p-type semiconducting film, which is expected from this device setup. It must be noted that this back gated setup for these devices never induced a complete switching on or off for the SWNTTFs. This is evident from the data as neither of the on or off states exhibited a plateau region where an increase (or decrease) in V_g resulted in no change to the drain current. Devices that were exposed to any larger gate voltages were susceptible to cracking the oxide beneath the electrodes or SWNTTF which results in gate leakage. Any devices showing gate leakage were incapable of any I_d-V_g measurements. Inefficient back gating is most likely the reason for not seeing the complete I_d-V_g curve with no I_{on} or I_{off} plateau for any films.

Although the back gating was not completely efficient, a general trend can be seen in the data. Increasing the SWNTTFs aspect ratio (L:W) resulted in an increase in the average I_{on}/I_{off} of devices (from I_{on}/I_{off} = 6 to I_{on}/I_{off} = 28). This I_{on}/I_{off} increase with respect to an increased aspect ratio is expected according to percolation theory with the SWNTs considered conducting sticks[87]. As the density remains constant between channels, metal nanotube percolation between electrodes is more likely to occur for wider geometries, which contributes to a higher I_{off}. It has been demonstrated through simulation and experimentation that fluctuations in on and off currents can be expected with random SWNTTF growth[74], explaining the variability observed between channels with identical dimensions. Nanotube bundling can also play a large role in determining I_{on} and I_{off} as current across a SWNTTF can be bottlenecked across single tubes. This will result in a large voltage drop over a small distance in the film, known as a voltage cliff. Any films exhibiting a voltage cliff will have a very low I_{off} compared to a film with a consistent voltage drop across it, leading to a large variation in the I_{on}/I_{off}.

2.3.2 pH Sensing

Changing the test solution between various buffered solutions is the simplest way to study the electrochemical effects occurring at the surface of the SWNTTF. In comparison to capturing large biomolecules (proteins, viruses, etc.) that have varying charge along their primary structure, ions are small molecules of constant charge. A constant surface charge density can be achieved for the SWNTTFs and substrate by varying the pH of the solution. With high control over the electrostatic nature of the environment, comparison between devices

becomes very straightforward and specific sensing mechanisms can be isolated. Exact pH test protocol can be found in *appendix B*.

In addition to biomolecule sensing discrepancies, literature shows that these discrepancies even exist between research groups regarding solution pH change and its effect on CNT sensors. Some have reported conductance *increases* with respect to increasing pH levels[88–90]. These conductance changes are typically attributed to the adjacent substrate surface producing a gating effect on the nanotubes. On the other hand, some research groups have observed the exact opposite trend occurring[53,65,91–95], where conductance increases with respect to *decreasing* pH levels. Electron transfer after adsorption of H^+/OH^- ions is a common explanation for this observed trend. Some reports have even shown that pH changes result in no electrical change to bare nanotubes[28]. Explanations for these discrepancies could be the amount of defects in the nanotubes and the numerous device fabrication methods involved. The overall structure of the defective SWNTTFs could potentially yield an opposite response than that of pristine tubes. This stems from the fundamental theory of whether or not the nanotubes have covalently linked functional groups or physically adsorbed ions on their surface. Device fabrication steps involving surfactants, acid washes and cleaning can all contribute to different interactions between the SWNTTF and ions in a pH experiment. However, there is no clear indication as to why so many reports have shown these contradictory pH dependent resistance responses.

For pH sensing, a time dependent response of these devices is required to justify claims regarding SWNTTF based devices being ideal biosensors for real-time sensing. Further, it is a

very simple way to determine when the successful addition of a new solution is in the microfluidic channel. Using this, a consistent incubation time for each sample is possible. *Figure 2.5* shows the time dependent I_d response to pH changes for a device at each aspect ratio at a constant V_d of 10mV.
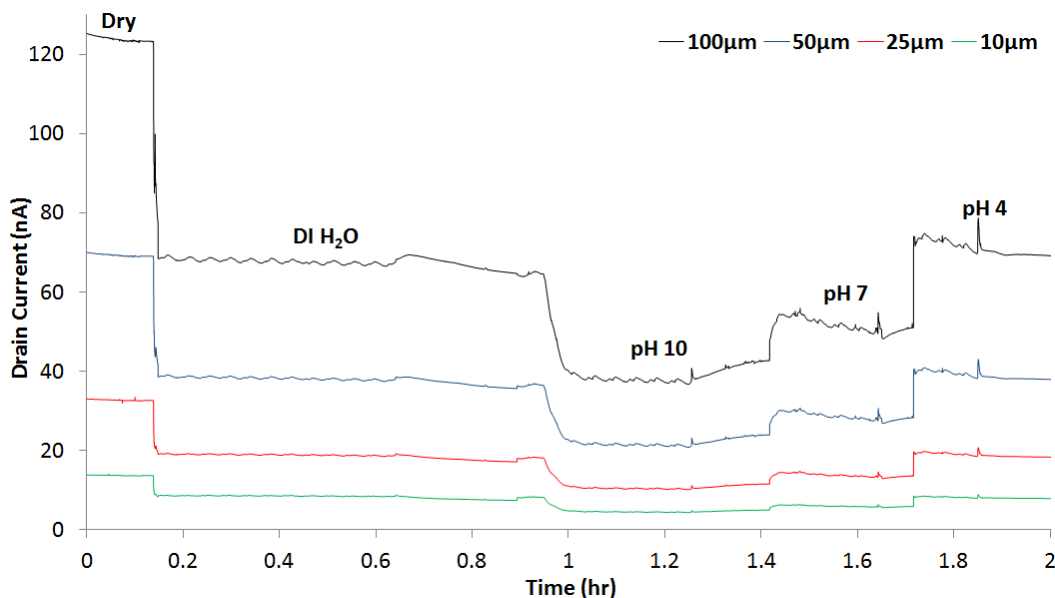
Figure 2.5: Time dependent current response to different pH conditions for one device at each aspect ratio.

Figure 2.5 demonstrates that these SWNTTF devices have a resistance dependence on solution pH. Beginning in the dry state, we see that a stable current is achieved almost immediately due to gases in ambient conditions requiring very little time to arrange on the surface of the nanotubes once a drain voltage is applied. Once DI H_2O is introduced into the channel, an immediate 60% decrease is observed in the drain current for each device. For the most part, this has been attributed to the H_2O surrounding the nanotubes altering the electric field and doping the pi network of the SWNTTF[70,96]. Theory as to why this always leads to a decrease in current is not fully understood. From the wet state, the devices then undergo the whole pH test.

A stepwise response can be seen when each subsequent pH condition is introduced into the microfluidic channel. It is clear to see that there is a resistance decrease with a decrease in solution pH. By analyzing the real-time current response of the SWNTTFs, it is clear that the nanotubes are capable of immediately sensing an electrochemical change in their environment. With stabilization times of a few seconds, these devices show promise for real-time biosensors.

It is worth noting that the periodic oscillation observed in the I_d-t curves for the devices are attributed to the peristaltic pump. The mechanism behind pumping involves the tube being pinched against the tube casing to provide fluid flow, which in turn creates a varying flow rate within the channel. With this in mind it is easy to understand the periodic oscillation in a film's current. Another contributor to noise that was observed during every I_d-t test is from external vibrations which can be seen at 0.65hrs, 1.25hrs, 1.65hrs and 1.85hrs. These external vibrations were caused by the movement required to switch the pump off once the incubation time was completed for each solution.

In each pH condition, the drain current was measured with respect to a change in the drain voltage. A -0.5V to 0.5V sweep was applied to one electrode while the other was held at ground. With no gate electrode there is a resulting uncontrolled nature of the solution potential which results in a non-linear drain current response for each film. In order to find the resistance of each film the linear portion about 0V of each I_d-V_d curve is used to create a linear I_d-V_d curve, which can be seen in *figure 2.6*.
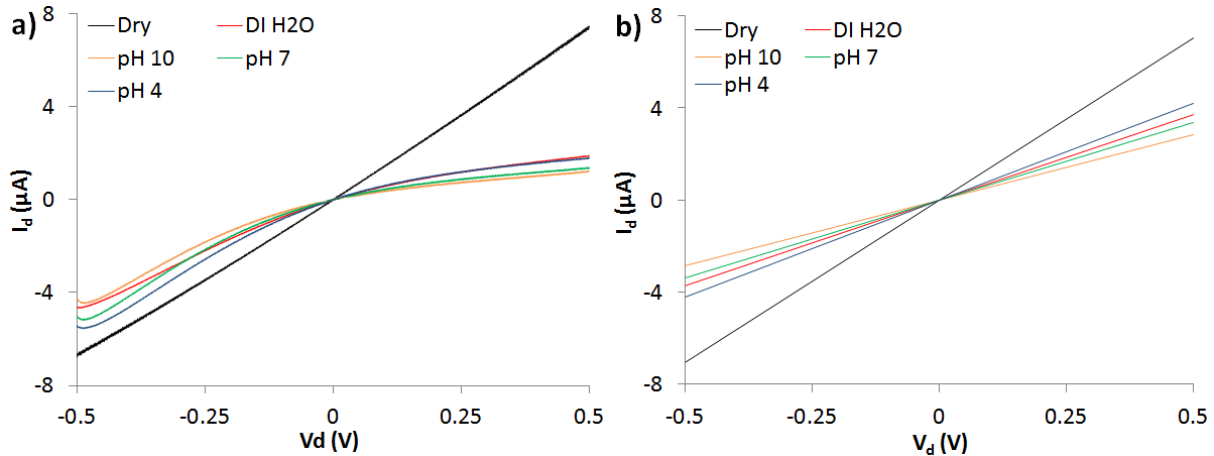
Figure 2.6: pH test results showing (a) raw I_d-V_d data measured and (b) fitted I_d-V_d data for resistance analysis.

Figure 2.6(a), which is the raw data I_d-V_d curve showing the non-linearity of SWNTF resistance. However, about 0V these curves did exhibit a linear response which was used to calculate film resistance for each device which can be seen in *figure 2.6(b)*. Due to this non-linear behaviour, it is imperative that resistance data used for subsequent analysis is taken from the same portion of each curve. It is of note that the direction of resistance change between different pH conditions is maintained throughout all of the raw I_d-V_d measurements. A linear representative I_d-V_d curve for one device at each aspect ratio can be seen in *figure 2.7*.
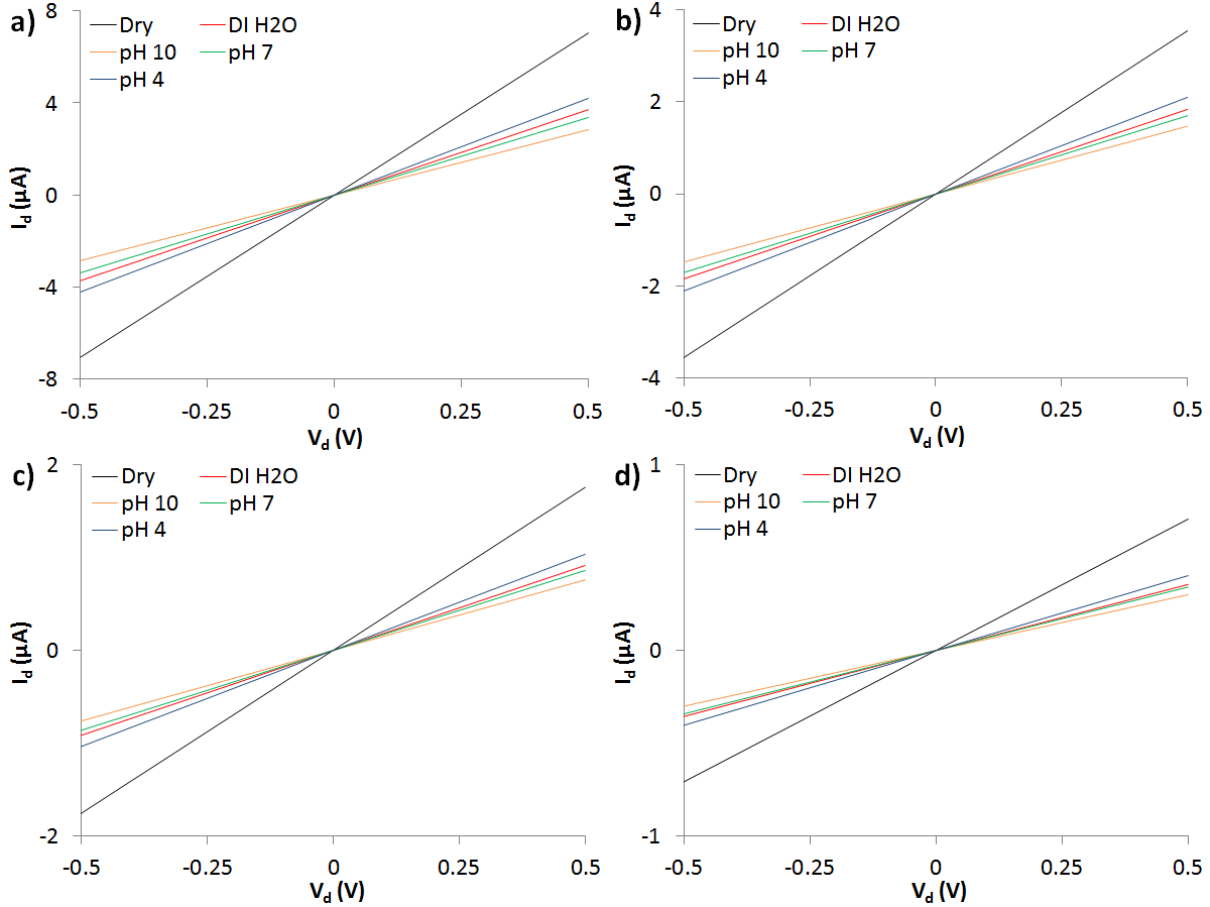
Figure 2.7: Representative Id-Vd curves in Dry state, DI H2O, pH 10, pH 7 and pH 4 for SWNTTF at aspect ratios (L:W) of (a) 1.5:1, (b) 3:1, (c) 10:1 and (d) 15:1.

Figure 2.7 shows consistent direction of resistance responses to pH change for every device measured. Current increases at a certain V_d indicate the SWNTTF's resistance is decreasing. The expected dry state resistance increase with respect to aspect ratio increase is observed from this data. Films with a 1.5:1 (L:W) aspect ratio in *figure 2.7(a)* showed an expected ten times decrease in current compared to films with a 15:1 aspect ratio in *figure 2.7(d)*. In order to fully comprehend all of the pH sensing data, statistical analysis must be completed on all devices. *Table 1* shows the average normalized to pH 10 resistance change ($\Delta R/R_o$) from pH 10 to pH 4 for all 8 devices at each film aspect ratio.

Channel Width (µm)	Average $\Delta R/R_o$ (%)	St. Dev (%)
100	14.69	0.51
50	11.92	0.63
25	14.30	0.88
10	15.82	0.99

Table 1: Average and standard deviation of SWNTTF normalized resistance change from pH 10 to pH 4 condition for each device aspect ratio.

There are two main conclusions that can be made after analyzing *table 1*. Firstly, there is a consistent average resistance change observed between the pH 4 and pH 10 conditions. For every device tested, there is an increase in resistance with respect to increasing pH, which is consistent with a number of literature reports. Secondly, we can see that there is no resistance change dependence on the aspect ratio of the film. This conclusion is vital to analyzing and understanding the subtle differences between bare nanotubes interacting with ions and bare nanotubes interacting with biomolecules, which will be discussed in *section 2.3.4*.

2.3.3 M13 Detection

After all pH testing was completed, the SWNTTFs were then used to detect various concentrations of M13 bacteriophage. Similar to pH testing, solutions containing biomolecules were sequentially introduced into the microfluidic channel following the protocol of previously reported experiments[20]. The complete protocol is described in *appendix B*. Akin to pH testing; the I_d of each film was measured with respect to a varying V_d in all biological conditions once a stable signal was reached. A representative measurement at each film aspect ratio can be seen in *figure 2.8*.
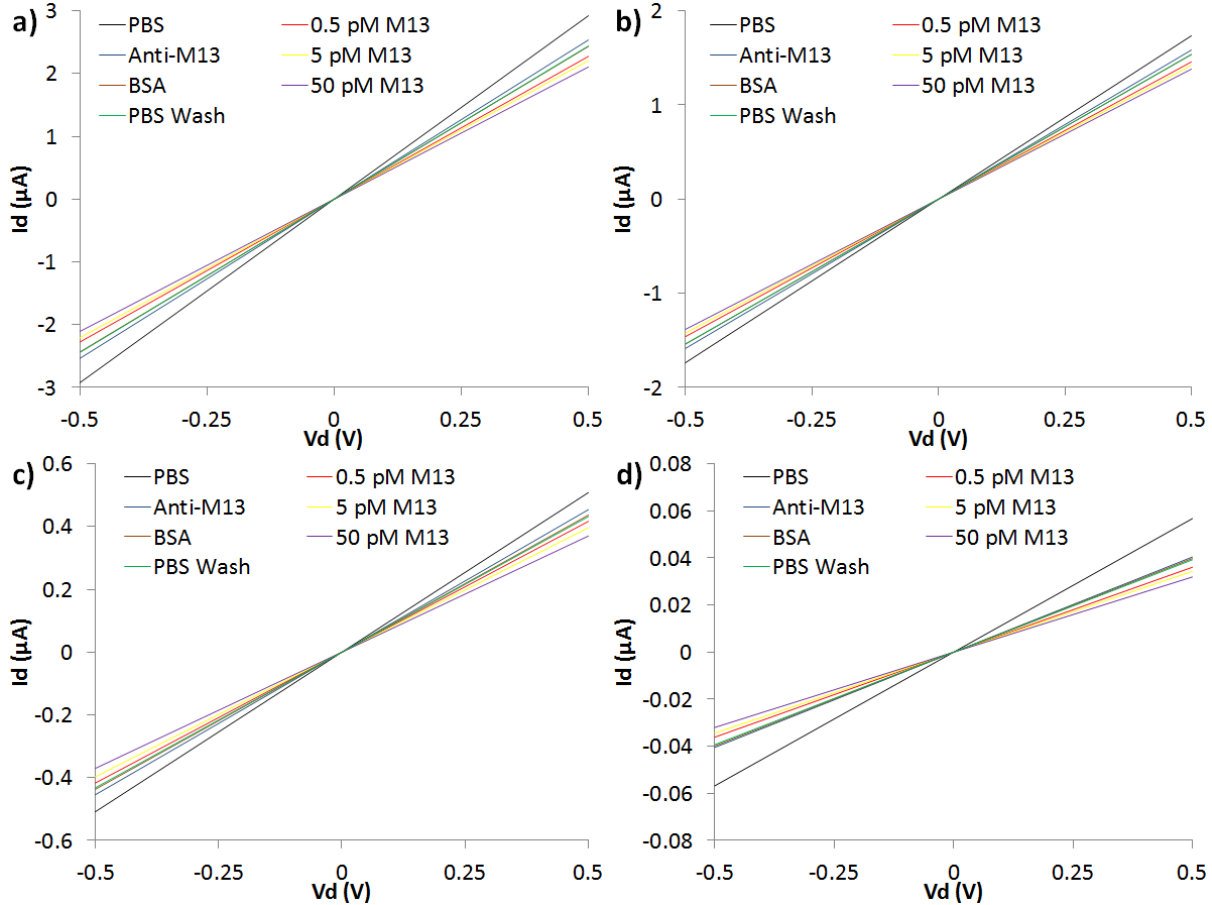
Figure 2.8: Representative I_d-V_d curves in 1x PBS, 100nM Anti pIII M13 Ab in 1x PBS, 1% BSA in 1x PBS, 0.5pM M13 in 1x PBS, 5pM M13 in 1x PBS and 50pM M13 in 1x PBS for SWNTTF at aspect ratios of (a) 1.5:1, (b) 3:1, (c) 10:1 and (d) 15:1.

Similar to pH sensing results in *figure 2.7*, *figure 2.8* shows the linear fitted I_d-V_d response from a film with each aspect ratio. Each sample solution was pumped through channel for 30 minutes prior to the pump being deactivated for resistance measurements to take place. The resistance change took place within minutes of the M13 bacteriophage introduction into the channel. This approximately follows the diffusion-capture theory simulation for one-dimensional nanowires mentioned in *section 1.3.2*. All aspect ratios showed this time-dependent response meaning that film geometry at this density does not affect required sensing time. During the M13 detection test, aside from the second PBS wash, every device was observed to have a resistance increase as each new sample solution was introduced

into the microfluidic channel. This observation follows reports in literature very closely where SWNT based devices incubated with biomolecules show resistance increases regardless of biomolecule charge[55]. In order to analyze the SWNTTF's response to different concentrations of M13 bacteriophage, *figure 2.9* and *table 2* show the normalized to PBS wash resistance change at each concentration of M13 bacteriophage with 8 devices at each film aspect ratio.
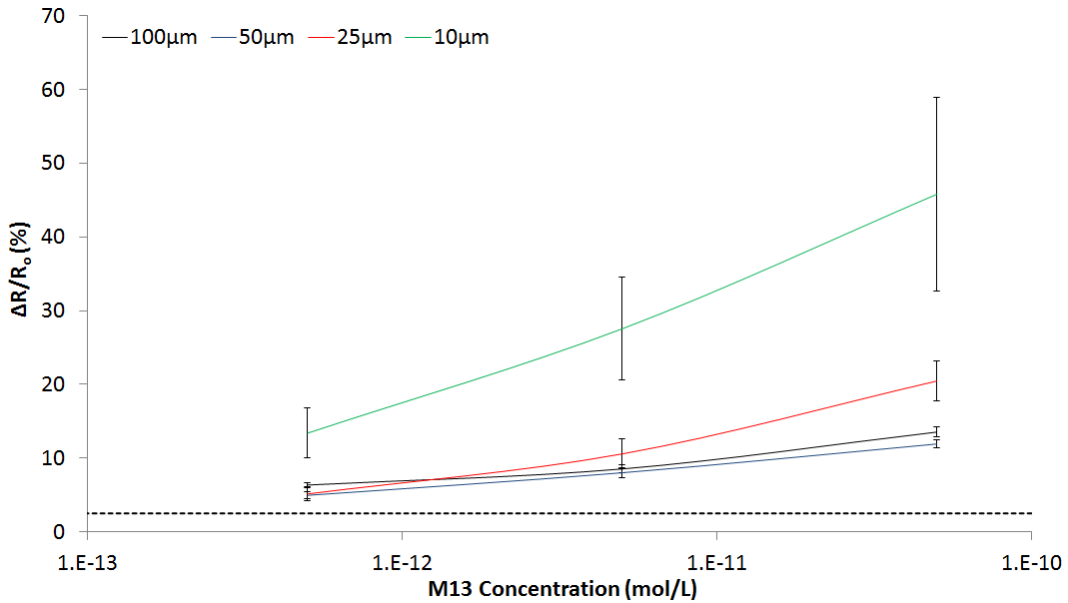
Figure 2.9: Average SWNTTF normalized (to PBS wash 2) resistance change at 0.5pM M13, 5pM M13 and 50pM M13 conditions in a semi-logarithmic plot for each device aspect ratio.

Channel Width (μm)	0.5pM M13		5pM M13		50pM M13	
	Avg ΔR/Ro (%)	St. Dev (%)	Avg ΔR/Ro (%)	St. Dev (%)	Avg ΔR/Ro (%)	St. Dev (%)
100	6.35	0.66	8.53	1.07	13.54	1.38
50	4.95	0.91	8.01	1.34	11.91	1.00
25	5.13	1.86	10.57	4.00	20.46	5.54
10	13.38	6.80	27.54	13.91	45.80	26.17

Table 2: Average and standard deviation of SWNTTF normalized (to PBS wash 2) resistance change at 0.5pM M13, 5pM M13 and 50pM M13 conditions for each device aspect ratio.

There are two significant conclusions that can be made from the statistical analysis of the SWNTTF's resistance change at different M13 concentrations. First, it is clear that the devices respond with an increasing resistance as the concentration of M13 increased. This is

expected as an increased amount of capture events should occur at higher bulk concentrations of M13. Second, there is a normalized resistance response dependence on the SWNTTF's aspect ratio or I_{on}/I_{off}. It was observed that an increase in aspect ratio resulted in a larger magnitude of response from the SWNTTF. However, this increased sensitivity to M13 also resulted in an increased variation in the average resistance change. These two points are very important when sensing mechanisms are discussed in *section 2.3.4*. Negative controls for this exact system have been previously reported[20]. In this work, it was shown that M13 capture events must take place in order for any response to be seen in the SWNTTFs resistance. If the anti-M13 pIII antibodies were blocked prior to being adsorbed onto the SWNTTFs or the pIII coat protein of M13 was removed, there was no response from the SWNTTF during tests.

It is important to confirm that biomolecules did indeed adsorb onto the surface of the SWNTTF after the M13 detection tests are complete. This confirmation will serve two main purposes. First, non-specific binding can be ruled out for the response to the M13 bacteriophage. It will give an idea of the protein surface coverage that occurs throughout all stages of the M13 detection tests. Second, it will help to understand and analyze the responses of the SWNTTFs during the sensing mechanism discussion in *section 2.3.4*. Subsequent to the M13 detection test the device was washed with PBS for 1 hour then DI H_2O overnight to ensure that all free floating biomolecules in solution are completely removed from the microfluidic channel. After this, the device was disassembled and the SWNTTF was imaged using AFM. *Figure 2.10* contains all information pertaining to the AFM image and section height analysis for a device *after* the M13 detection test was completed.

41
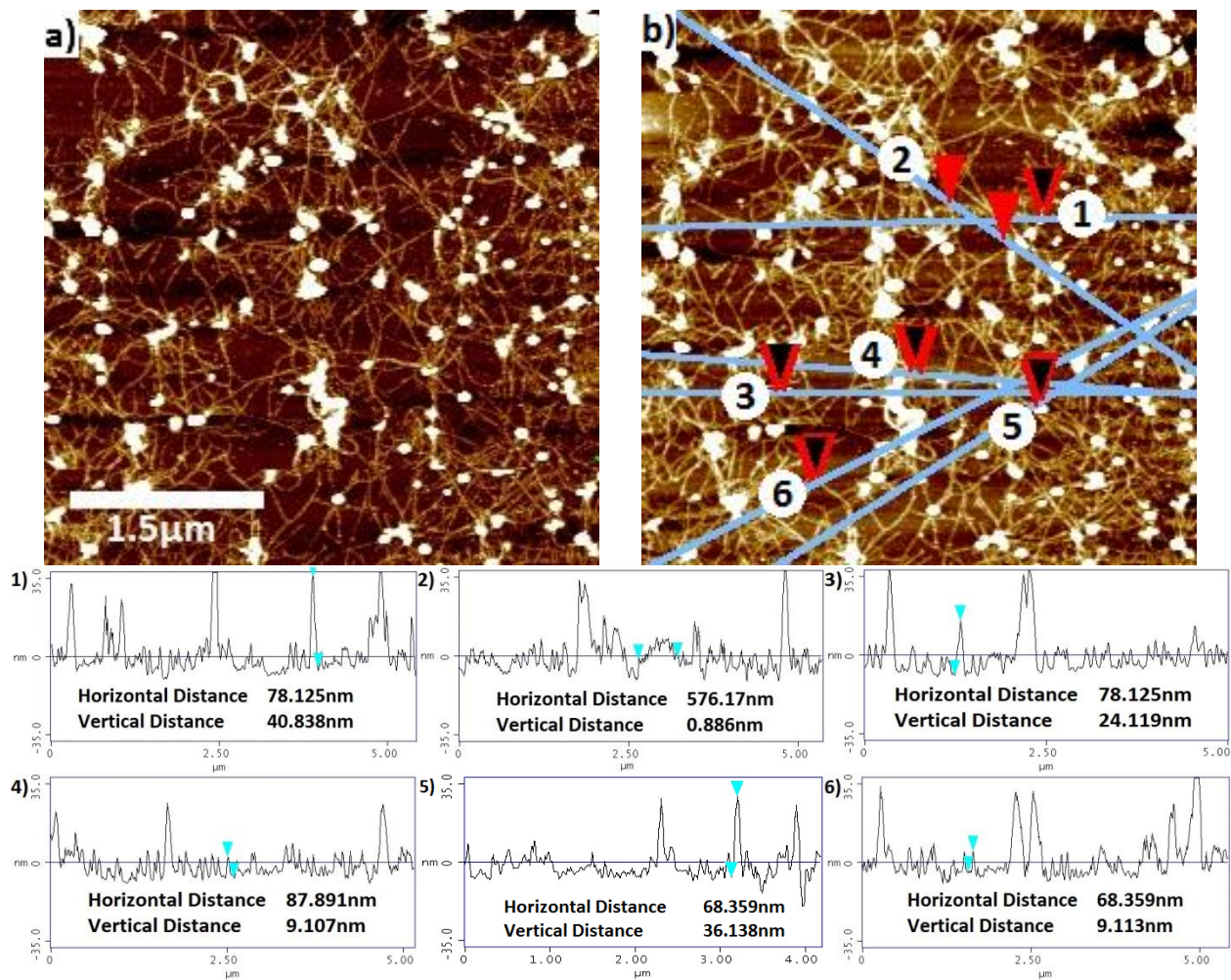
Figure 2.10: AFM characterization of SWNTTF after anti-M13 Ab, BSA and M13 bacteriophage adsorption including (a) the original AFM image coated SWNTTF, (b) the AFM image indicating the location of height measurements along the image section (blue lines) and (1-4) the height measurements along each section.

Figure 2.10(a) shows the original AFM image of a SWNTTF in the middle of the microfluidic channel after the M13 detection test. *Figure 2.10(b)* is the same image showing the sections analyzed indicated by the blue lines and the exact point at which it was done indicated by the arrows. The height profile and measurements performed between the two arrows are shown in *figures 2.10(1)-(6)*. By examining *figure 2.10* it is clear that the substrate and SWNTTF are indeed coated with at least a layer of biomolecules subsequent to the M13 detection test. Even without section analysis, the tubes appear larger and the surface of the substrate and

tubes appear to be much rougher compared to the tubes in *figure 2.3(a)*. The two arrows in

figure 2.10(2) travel along an isolated nanotube demonstrating the increased roughness of the

nanotubes surface. The image also shows that junctions were seen to lose their tube like

properties as they became spherical in nature. Section analysis of this SWNTTF shows the

average diameter of nanotubes isolated on the substrate increased from 1.8nm-3.6nm to

approximately 10nm. A similar increase was also seen at the tube junctions. Further, the SiO_2

roughness was seen to increase by a few nanometers compared to *figure 2.3(a)* indicating that

biomolecules, most likely being BSA, are adsorbed everywhere on the device surface.

2.3.4 On the Dominant Sensing Mechanisms in SWNTTF Chemiresistors

Section 1.3 proved there have been a number of mechanisms proposed to explain and

understand the electrical response of SWNT based devices in varying electrochemical

conditions. Between the sensing mechanisms that were discussed, there lies a great deal of

overlap that makes isolating the mechanisms very difficult. Further, some of the sensing

mechanisms theoretically affect the nanotubes electrical properties in opposite directions. As

aforementioned, there have been many studies that have used at least one of these

mechanisms to explain their results. With a number of mechanisms available for explanation,

researchers are able to be very selective in their device analysis, which is the fundamental

reason for debate still taking place regarding the sensing mechanisms[26]. This is the primary

reason that a direct comparison between a device's responses to pH changes and M13

detection was pursued for this study. Monitoring the electrical response of the SWNTTFs in

both conditions will help to understand the fundamental differences between each scenario.

With this information it is possible to reach some conclusions relating to the dominant sensing mechanisms for SWNTTF electric sensors. The statistical analysis of the test results from *section 2.3.2* and *section 2.3.3* which relate the dry state I_{on}/I_{off} to the normalized resistance change for sensing tests can be seen in *figure 2.11*.
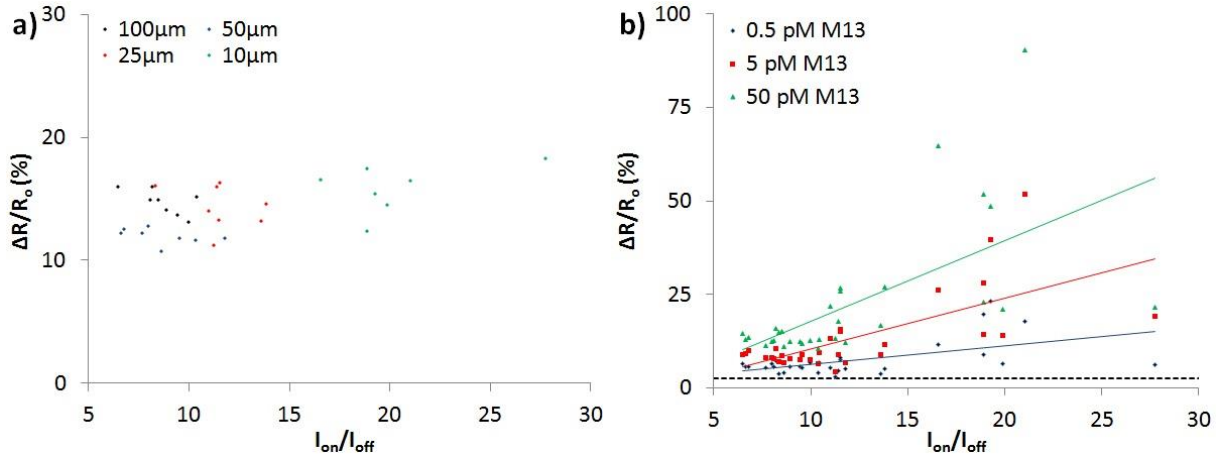
Figure 2.11: Correlation between each SWNTTF's I_{on}/I_{off} and its (a) pH 10 normalized resistance change from pH 10 to pH 4 and (b) PBS wash normalized resistance change for all M13 Bacteriophage concentrations.

Figure 2.11(a) shows the pH 10 normalized resistance changes to pH 4 *versus* the I_{on}/I_{off} for each of the SWNTTFs tested. *Figure 2.11(b)*, on the other hand, shows the PBS normalized resistance change to all M13 concentrations *versus* the I_{on}/I_{off} for each SWNTTF. These graphs show two very important things. First, a change from pH 10 to pH 4 showed no dependence on the I_{on}/I_{off} for the SWNTTF. This means that regardless of how susceptible the SWNTTF was to back gating in the dry state, each film showed very similar resistance changes from the pH 10 state to the pH 4 state. Second, and in contrast to the pH tests, the SWNTTFs did show a normalized resistance dependence on the I_{on}/I_{off} for each concentration of M13. This relationship was further amplified with increased concentrations of M13 bacteriophage.

Common explanation for resistance change in SWNTTFs involves alterations to the electric field surrounding the nanotubes inducing conductance changes within the film, referred to as capacitive coupling[29,31,32,51,62–64] or electrostatic gating[55–57]. The electric field is transmitted to the nanotube by ions that form the ionic double layer around the tube[57], varying the surface charge density and surface potentials for different chemical environments. These mechanisms are governed by the relationship seen in *equation 9*:

$$\Delta V = \frac{\Delta Q}{C_{Total}} \qquad (9)$$

Where ΔQ is the surface charge per unit area of the nanotubes, ΔV is the potential difference created by the addition of charged species and C_{Total} is the total capacitance of the nanotube-double layer capacitor[63]. The total capacitance of the system can be broken up into the series addition of the two capacitors seen in *equation 10*:

$$\frac{1}{C_{Total}} = \frac{1}{C_Q} + \frac{1}{C_{DL}} \qquad (10)$$

Where C_{DL} is the double layer capacitance and C_Q is the quantum capacitance of the nanotube. In the solution phase, C_{DL} is at least an order of magnitude larger than C_Q, meaning that the quantum capacitance dominates C_{Total}[63]. The quantum capacitance is a function of the density of states (DOS) of the nanotubes, meaning that changes to the DOS due to electrochemical perturbations results in conductance changes within the SWNTTF. As each device has a similar SWNT density, a certain test condition should yield identical surface potential and charge density per length of tube regardless of channel dimensions. This leads to the conclusion that if the dominant sensing mechanism relies on the electric field surrounding

the nanotubes, devices with higher I_{on}/I_{off} should yield greater resistance changes and increased sensitivities.

The SWNTTFs showed no resistance change dependence on I_{on}/I_{off} during the pH tests. Chemical doping is thought to be the dominant mechanism for pH response as H^+/OH^- ions adsorb to the surface of the SWNT. This involves partial electron transfer between a nanotube and charged molecule taking place at the nanotube's surface[51]. Experiments have proven that resistance changes of the nanotube correspond to the redox state of the molecule in contact with the nanotubes rather than the overall charge of the molecule[49]. Being p-type in nature, nanotubes that interact with oxidizing molecules show an increase in conductance resulting from depletion of electrons from the valence band, and vice versa for reducing molecules. This explains H^+ adsorption occurring at low pH's resulting in a decreased network resistance while OH^- adsorption occurring at high pH's resulting in an increased network resistance.

To completely rule out electrostatic gating as a dominant mechanism for pH response, the surface properties of SiO_2 must be taken into account. It is well known that SiO_2 surfaces are negatively charged for all the pH values used in this study[97]. As solution pH increases, the surface of SiO_2 will become increasingly negative as additional OH^- ions in solution deprotonate silanol groups. This effect emulates a negative back gating effect on the SWNTTF from the SiO_2 surface resulting in a decrease in p-type semiconducting material resistance. Although this surface charging is taking place, the opposite trend seen in data concludes that electrostatic gating has a minimal effect on the nanotube's electrical properties in these pH sensing tests.

The M13 detection test, however, showed resistance changes that were dependent on I_{on}/I_{off} of the SWNTTF. Further, previous studies have shown that if there is no interaction between the anti-M13 Ab and M13 bacteriophage, the SWNTTF exhibits no noticeable electrical response[20]. This signifies that capture events occurring near the surface of the SWNTTF are the reason for electrical detection of M13. With a monolayer of biomolecules adsorbed onto the SWNTTF after BSA incubation shown in *figure 2.10*, an increased distance and permittivity exists between the surface of the nanotubes and the captured virus. This suggests that a few, if not all, of the mechanisms of electrical detection of biomolecules[26] are at play as direct chemical doping of the nanotubes is not possible. However, because of a clear dependence resistance changes had on the I_{on}/I_{off} of the SWNTTFs, it is postulated that response due to the electrostatic gating mechanism is significant.

It is important to note that the dependence of the resistance change on the concentration of M13 in *figure 2.9* is logarithmic. This is not the expected theoretical relationship between these two variables if electrostatic gating is the only mechanism of sensing. Conductance changes strictly due to electrostatic gating should have an exponential dependence on M13 concentration. The drain current of SWNTTFs exhibit an exponential dependence on the gate voltage within the subthreshold region, following the subthreshold slope. During the M13 detection test each subsequent concentration of M13 increased by 10 times, meaning that devices should have experienced a corresponding 10 times response if electrostatic gating was the only mechanism of sensing. One potential reason for this non-exponential relationship between these variables is a saturation of receptor molecules. If this is the case, the SWNTTF may still have an exponential response but this information cannot be

47

extracted due to saturation showing non-exponential behaviour. Another potential explanation for these observations is the device is operating outside of the subthreshold region. In the wet state with a number of biomolecules adsorbed onto the SWNTTF's surface, current measurements already show significant switching of the SWNTTF's electrical conductance. With this in mind, an exponential relationship between the normalized resistance response and the M13 concentration should not be expected.

The variation in M13 detection results observed in narrow channels is understandable when junction resistance and percolation theory in a SWNTTF are considered. Recent work has demonstrated that resistance at tube junctions dominates overall network resistance for pristine nanotube films[33,98,99]. Further, according to percolation theory, a 10µm wide channel has less pathways connecting the source and drain electrodes compared to a 100µm wide channel with the same nanotube density[84]. This means that although all channels have the same SWNTTF density, narrow channels are more susceptible to a capture event occurring on a pivotal nanotube or junction. Therefore, depending on the location of the capture event, a higher aspect ratio film could be greatly affected or not affected at all.

In light of this analysis, a different substrate was used to determine the effect protein adsorption has on the dominant sensing mechanisms during a pH test. The pH test is performed both before and after coating the SWNTTFs with a layer of proteins (anti-M13 Ab, BSA and M13 bacteriophage). *Figure 2.12* shows representative I_d-V_d responses to pH change from pH 10 to pH 4 from the SWNTTF's both with and without a biomolecule coating.
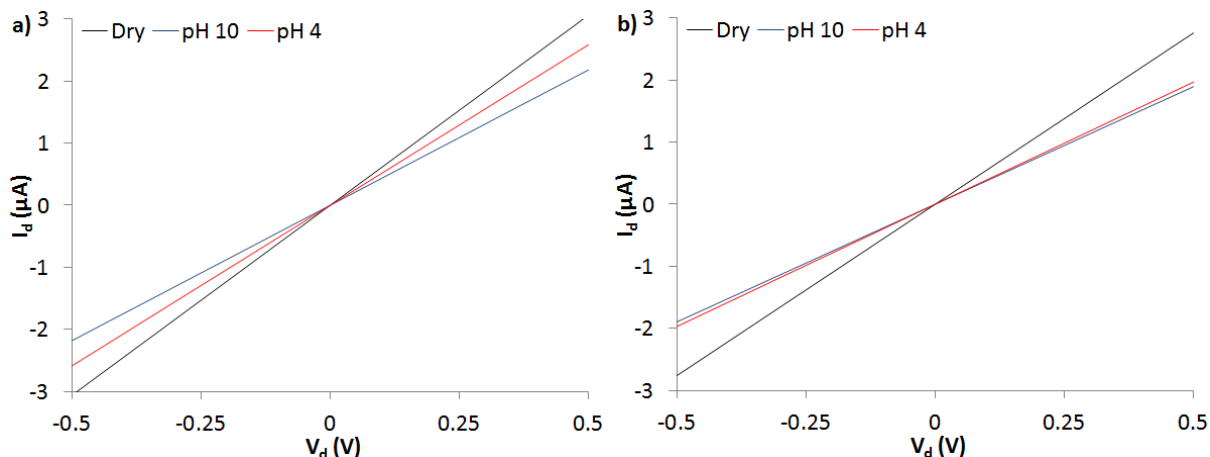
Figure 2.12: Representative SWNTTF I_d-V_d measurements for a 1.5:1 aspect ratio film (a) before M13 detection test and (b) after M13 detection test.

The main observation made from the analysis of *figure 2.12* is that there is a supressed resistance response to pH changes when biomolecules are adsorbed on the surface of the SWNTTF. *Figure 2.13* gives a comprehensive look at the change in response to the pH test before and after biomolecule adsorption for a number of SWNTTFs.
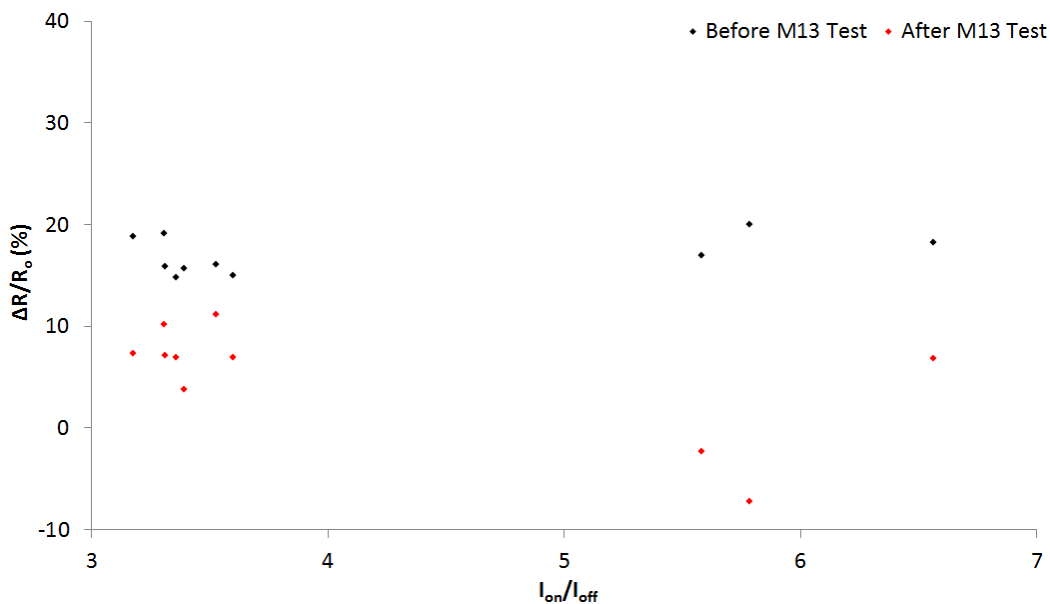
Figure 2.13: pH 10 normalized resistance change to pH 4 versus I_{on}/I_{off} for each device both before and after M13 detection test.

With information regarding the pH 10 normalized resistance changes to pH 4 for devices before and after biomolecule adsorption, *figure 2.13* points to a few qualitative conclusions.

49

Firstly, it confirms that there is definitely a supressed resistance response to pH for devices that are coated in a layer of biomolecules. The two possible reasons that explain the change in response from the SWNTTF can be better understood after analyzing *figure 2.14*, which shows a schematic difference between the bare nanotube and the biomolecule coated nanotube in pH 10 solutions.
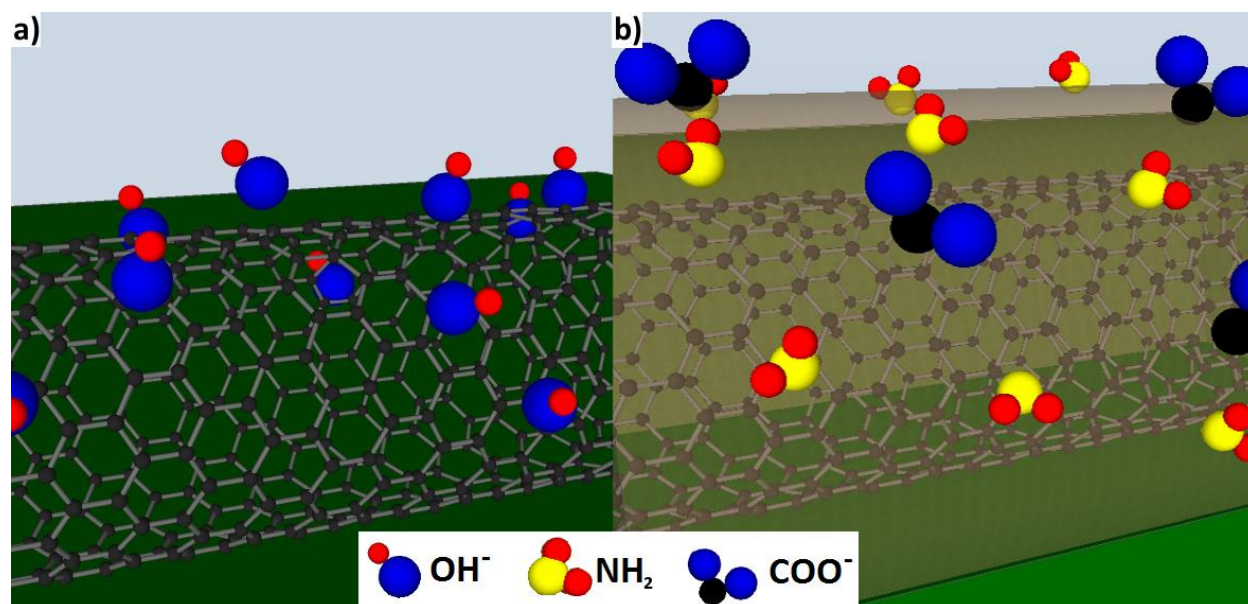
Figure 2.14: Schematics demonstrating the difference between a (a) bare SWNT in a pH 10 buffer and (b) protein (transparent layer) coated SWNT in a pH 10 buffer.

Figure 2.14(a) shows the surface of a bare SWNT while *figure 2.14(b)* shows the surface of a protein coated SWNT, both in a pH 10 buffer. For the bare nanotube case, it is clear to see that the surface charge determining ions in solution have complete access to the surface of the SWNT. The bare nanotubes are highly susceptible to electron transfer from the H^+/OH^- ions in solution because of this. In the protein coated nanotube case, however, the decreased response can be attributed to the layer of proteins adsorbed on the nanotube's surface hindering the diffusion of H^+/OH^- ions to the surface of the nanotubes. Along with the diffusion

hindrance, some SWNT surface sites that were accessible to ions during the bare tube pH test are occupied by proteins once it is coated.

Another potential reason for response suppression is the electrochemical interaction between H^+/OH^- ions and the proteins on the surface of the SWNT. With the majority of the surface being coated with BSA, which has an isoelectric point of 4.7[100–103], the overall effect of these charged proteins on the SWNTTF must also be taken into account. At pH 4 the protein is slightly positively charged as additional H^+ ions in solution protonate amine groups of certain amino acids. The opposite of this effect occurs at pH 10 where carboxylic groups on amino acids are deprotonated and the overall charge of the protein is negative, which is depicted in *figure 2.14(b)*. The resistance change observed in the SWNTTF is opposite to what is expected in these pH conditions if electrostatic gating is dominant. However, this could indicate an increased significance of electrostatic gating which would thereby decrease the observed electrical response due to direct chemical doping of H^+/OH^-. It is of note that two devices were observed to have a resistance decrease with pH increase, which was opposite to all pH testing done previously. Simulation and experimentation have shown that single tubes and junctions have been shown to bottleneck current in low density films[74]. This means that specific interactions at single nanotubes or junctions in the SWNTTF can significantly control the overall conductance of the film. If gating is the dominant mechanism at this point, it would be possible to see a lower resistance at pH 10.

2.3.5 Device Calibration

On top of successful detection experiments, an additional goal of this work was to find experimental data that could be used for device calibration. It was hypothesized that this could be done by finding a relationship between each device's resistance change at specific M13 concentrations and either its dry state switching properties or pH response. Semiconducting nanotube switching during experimentation is thought one of the main reasons for device response. With this information, quantitative values pertaining to a back gate response or charge density change at different pH levels could be correlated to specific responses from different M13 concentrations.

Section 2.3.4 contains information and analysis that can be used to potentially find a calibration for the devices. One important conclusion made in this section of concern to calibration is the difference between the dominant sensing mechanism for the pH and M13 response. Chemical doping was seen to be the dominant sensing mechanism during pH testing, while electrostatic gating was observed to be the dominant sensing mechanism for the devices response to different M13 concentrations. In light of this, no real correlation could be made between the surface charge density at different pH levels and the response to different M13 concentrations.

The normalized resistance change, on the other hand, did show some dependence on the I_{on}/I_{off} for the devices at all concentrations of M13. On average, 15:1 aspect ratio SWNTTF devices showed the highest I_{on}/I_{off}'s as well as the highest resistance responses to M13 capture events. Individual devices, on the other hand, did not exactly follow this trend as some films

with high I_{on}/I_{off}'s yielded some of the lower end resistance changes for a specific SWNTTF geometry. Because of this, it is difficult to use the dry state I_{on}/I_{off} for device calibration as resistance change depending on M13 concentration yielded a significant amount of variance, especially as the aspect ratio increased.

In light of this, individual channels were then studied in order to determine whether or not another method of pre-test calibration can be performed on the devices. In order to prepare each device for the M13 detection test, anti-M13 Ab and BSA are adsorbed onto the surface of the films. A relationship between the normalized resistance response to initial biomolecule adsorption and the normalized resistance response to M13 capture events for each film can be seen in *figure 2.15*.
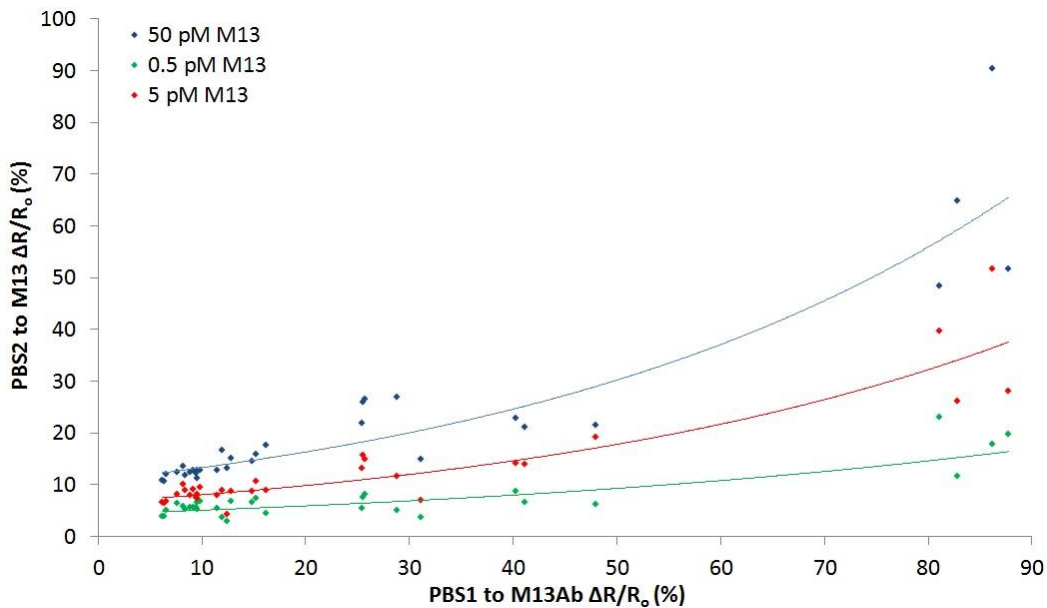
Figure 2.15: PBS normalized resistance response to anti-M13 antibody versus PBS normalized resistance response to all M13 concentrations.

It is clear from *figure 2.15* that regardless of pH response as well as I_{on}/I_{off}, the films that showed the greatest response to the anti-M13 Ab also showed the greatest responses to M13

capture events. This relationship shows a potential method that can be used prior to virus detection to relate a specific normalized resistance change to an unknown virus concentration. Each device's resistance showed a logarithmic dependence on the M13 concentration. Thus, a logarithmic fitting was used to determine the coefficients for each device's response during the M13 detection test. With this, the normalized resistance measured during a detection test can be related to the unknown M13 concentration depending on how it responds to the anti-M13 Ab. As each device showed a logarithmic dependence on M13 concentration, the expected relationship can be seen in *equation 11*:

$$\frac{\Delta R(M13)}{R_o} = a * \log_{10}([M13]) + c \qquad\qquad (11)$$

Where $\Delta R(M13)/R_o$ is the measured PBS normalized resistance change, [M13] is the concentration of M13 bacteriophage in M, and a and c are coefficients that are dependent on the normalized resistance change to the anti-M13 Ab. These coefficients were each plotted against the normalized resistance change to anti-M13 Ab, which can be seen in *figure 2.16*.
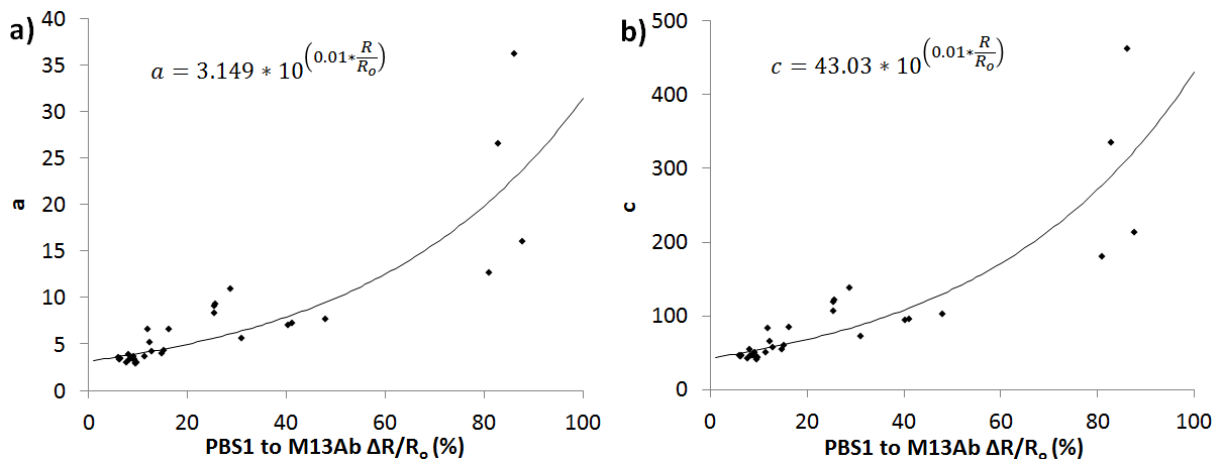
Figure 2.16: Plots showing the (a) a coefficient's and (b) c coefficient's dependence on the PBS normalized resistance change to anti-M13 Ab.

The scatterplots in *figure 2.16* show how the coefficients from *equation 11* depend on the device's response to the anti-M13 Ab as well as a fitted equation of this dependence. With this experimentally determined information, a relationship between the resistance response to anti-M13 Ab and the measured resistance response to an unknown M13 concentration can be formulated. *Equation 12* and 13 show this relationship:

$$[M13] = 10^{\left(b*\frac{\Delta R(M13)}{R_o}-13.66\right)} pM \qquad (12)$$

$$b = 3.149 * 10^{\left(0.01*\frac{\Delta R(Ab)}{R_o}\right)} \qquad (13)$$

Where $\Delta R(M13)/R_o$ is the normalized resistance change due to M13 capture events, $\Delta R(Ab)/R_o$ is the normalized resistance change due to anti-M13 Ab adsorption, and b is a constant determined experimentally for each device prior to the M13 detection test. With this, resistance responses from unknown M13 solutions can be correlated to a specific concentration by first measuring the device's response to the anti-M13 Ab.

Although this experimentally determined relationship that can be used to calibrate an individual device, it is only good for preliminary use. Further experimentation must be completed in order to decrease the amount of variance from the calibration curve. Also, as this is a qualitative way to determine a calibration curve, study must be completed towards finding a quantitative correlation between the resistance response and M13 concentration. The total number of captured M13 is still not able to be determined with this technique. To this end, a theory that can relate the effect of one captured M13 virus to a specific change in resistance is required.

2.4 Conclusions

This work demonstrates the reproducibility of CVD grown SWNTTFs used as the transducing component in chemiresistor biosensors. The study involves determining the underlying ionic and biological sensing mechanisms in 32 parallel, isolated and low tube density SWNTTF electrical biosensors. The effects device geometry has on the SWNTTF's dry state electrical properties as well as their sensing capabilities were studied.

Device analysis demonstrates chemical doping to be the dominant mechanism of sensing as pH level is changed. The surface sites available for H^+/OH^- adsorption as well as the ion's reducing/oxidizing nature are the principal reason for this observation. Further, it was observed that regardless of the I_{on}/I_{off} or the aspect ratio of the film, there was no change between the normalized resistance responses of the SWNTTFs. This rules out electrostatic gating contributions as films that were more susceptible to dry state gating showed no difference in response to pH changes.

Using the same devices for M13 bacteriophage detection, isolating a single sensing mechanism is difficult due to the complex nature of electrochemical interactions between nanotubes and biomolecules. Although chemical doping can play a role in the detection of a capture event, the dominant mechanism of sensing is determined to be electrostatic gating. M13 response dependence on a SWNTTF's I_{on}/I_{off} demonstrates that SWNTTFs more susceptible to dry state switching show the highest resistance changes as capture events occur. A linear range of these devices is unknown as the normalized resistance change *versus* M13 concentration show a logarithmic dependence.

Investigating the devices response to pH changes after biomolecule adsorption shows a decreased response to pH changes in solution with some cases even showing an opposite response. Hindered diffusion of H^+/OH^- ions to the SWNTTF's surface due to required transport through a layer of adsorbed proteins is the main cause of this response change. The effect of protein charge at specific pH levels also becomes more significant as some devices showed an opposite change in film resistance.

This study does not allow for calculation of the exact number of virus capture events that occurring on the surface of the SWNTTF. Contributions from multiple sensing mechanisms, which vary in response magnitude and direction for SWNTTFs or capture molecule saturation, are potential reasons for this. This study proves that there exists a relationship between the resistance response of the SWNTTF devices to anti-M13 antibody and M13 capture events, regardless of the dominant sensing mechanism. With this experimentally determined data, preliminary device calibration is achieved, which allows for calculating the bulk concentration of M13 bacteriophage in solution depending on the device's resistance response.

Increasing the aspect ratio of the low density SWNTTF from 1.5:1 to 15:1 (L:W) increases the sensitivity of the device. A single or a few nanotubes/junctions are likely to determine overall film resistance in higher aspect ratio SWNTTFs according to percolation theory. Further, the SWNTTFs electrical properties are more reliant on semiconducting nanotubes in higher aspect ratio films. Both of these factors greatly contribute to the increased sensitivity of the 15:1 SWNTTFs. An increased response variance also occurs in higher aspect ratio devices due to

this. Along with SWNTTF density, device geometry must be considered during prototype design in order to optimize the device's sensitivity as well as reproducibility.

Experimental limit of detection of M13 bacteriophage for all devices is 0.5pM, while theoretical limits of detection are approximately in the tens of fM levels for higher aspect ratio SWNTTFs. This shows that a simple approach to biomolecule using SWNTTF based chemiresistors are still capable of detecting sub-nanomolar concentrations of biomolecules.

2.5 Future Work

2.5.1 Device Calibration

Although a significant correlation was observed between a device's initial response to biomolecule adsorption and subsequent capture events, more work must be done towards quantitatively determining the exact concentration of analyte in solution. This is very important for the future commercialization of chemiresistive SWNTTF biosensors. A comprehensive study regarding a variety of SWNTTF densities and their responses to both antibody adsorption and capture events is required to find a calibration curve that is capable of accurately predicting the concentration of analyte in solution. This calibration curve must also be tested using unknown target analyte concentrations so that its predicting power can be improved.

Determining the amount of captured analyte on the surface of the SWNTTF, on the other hand, is a very important measurement regarding the underlying sensing mechanisms responsible for the devices electrical response. M13 detection tests at lower concentrations as well as smaller increments between concentrations must be completed to fully understand the

mechanisms at play. Further, as complete antibody saturation possibly occurred during this study, M13 capture events must be studied using adsorption isotherms to confirm if this is indeed happening. Knowledge of the total amount of captured analyte on the surface of the film would be helpful to determine the overall effect that a single capture even has on the electrical properties of the SWNTTF. With this information, quantitative analysis of the sensing mechanisms responsible for the electrical response of the films can be completed.

2.5.2 Receptor modification

The protocol used in this study to decorate the transducing SWNTTF with receptor molecules only involved random physisorption. Although this was a very simple technique capable of detecting pM concentrations of analyte, controlling this interaction between the receptors and transducers is of great importance. Random receptor adsorption on the nanotube's surface can result in an unfavourable orientation regarding the region of the antibody that is responsible for capture events. This could be a part of the reason for saturation as, although a high concentration of antibodies were adsorbed onto the SWNTTF, only a fraction of them may be capable of capturing the analyte. Further, this randomness introduced in step 1 of the test protocol could also be a reason for the inability of these devices to quantitatively measure the captured viruses. Future work that could help to solve these issues involves controlling the orientation of the receptor molecules by somehow modifying them to have the heavy chain adsorb/bond to the surface of the nanotubes. Functionalization of both the nanotubes and the receptors could lead to realizing a system with better receptor control.

2.5.3 Device Modifications

With any prototype fabrication, changes are continuously made to the overall device in order to realize an optimal system. For this system, the first of these changes involves optimizing liquid delivery to the microfluidic channel. The pressure/flow rate fluctuations observed during all tests is not desired. Using a syringe pump set up with a constant flow rate would allow for clean real-time measurements of capture events occurring. With improved sample injection equipment a lot of information can be gathered regarding the diffusion capture theory mentioned in *section 1.2.3*.

A lot of additional information can be gained if gating properties of the SWNTTFs are studied during these experiments. This modification would require incorporating a liquid gate into the microfluidic channel or a back gate in the chip carrier. This would allow for more accurate measurements of I_{on}/I_{off} prior to sensing experiments. Further, study of the shape of the I_d-V_g curve at each stage of M13 detection test would help to further understand the sensing mechanisms at play and could lead to a quantitative device calibration. Finally, having the ability to gate the SWNTTF during a sensing experiment would allow for the study of an optimal sensitivity in the subthreshold region.

2.5.4 Additional Testing and Analysis

During experimentation, some very interesting measurements were taken that require additional testing in order to fully understand them. The first unexpected measurement was the non-linear resistance observed in the I_d-V_d curves for every device tested in a liquid

environment. More worrisome observations involve the non-linear response being asymmetric about V_d = 0V as well as devices showing inconsistencies in this asymmetric behaviour. Some devices would show logarithmic behaviour at positive voltages and somewhat exponential behaviour at negative voltage, while other devices would have the exact opposite shape. In a system that has no potential control in solution (via a liquid gate), this non-linear behaviour is expected. This setup results in an inconsistent potential seen at the SWNTTF-buffer interface, which in turn will affect the tubes within the film differently. Controlling the liquid potential with a gate electrode could help to control the response of these devices.

3. BNP detection using PET based SWNTTF Biosensors

3.1 Introduction

Recent scientific meetings stated the great importance of detecting brain natriuretic peptide (BNP) in blood in a point-of-care and real-time manner. It is extremely useful as a prognostic marker for the early detection of heart failure and its differentiation from other diseases with similar immediate symptoms[104]. BNP is a neurohormone secreted by the left ventricle of the heart in response to blood pressure decreases or increased systematic vascular resistance[105]. The 32 amino acid sequence, structure and binding locations for the majority of receptor molecules of Human BNP can be seen in *figure 3.1*.
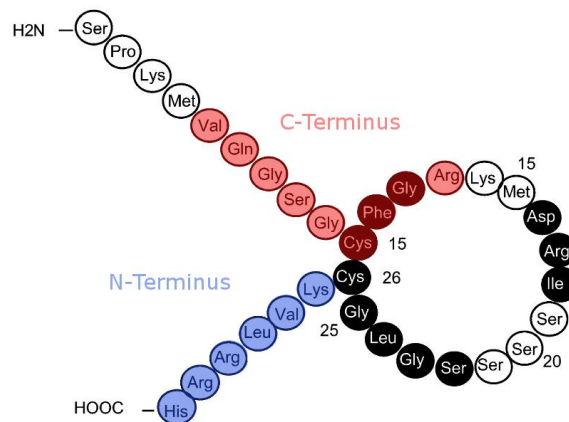
Figure 3.1: Schematic showing the structure and sequence of the 32 amino acid BNP molecule as well as the C-(red) and N-(blue) terminus binding locations for receptor molecules[106].

Figure 3.1 shows information pertaining to the structure, size and binding locations for receptor molecules on the human BNP molecule. It has been proven that there exists a direct correlation between elevated concentrations of BNP in the blood (> 500 pg/mL) and the severity of heart failure symptoms in patients. In addition, a gray zone (100 – 500 pg/mL) exists where elevated plasma BNP levels cannot be attributed to heart failure but could still lead to

the early prognosis of decompensation[107]. Individuals who have experienced any type of heart failure also experience fluctuating plasma concentrations of BNP, especially if another heart failure event is close to happening. This alone justifies the requirement of a point-of-care BNP monitoring system capable of real-time detection.

Current Food and Drug Administration (FDA) approved immunoassays for plasma BNP detection are optically based. These assays must also be carried out in medical laboratories or emergency rooms as they require trained personnel for sampling as well as bulky and expensive instruments for characterization[108]. Point-of-care devices to date are limited to use in emergency rooms due to their sample volume requirements. Household devices, on the other hand, would allow outpatients of heart failure to periodically monitor their own BNP levels (akin to a diabetic monitoring glucose levels) in order confidently determine the likelihood of heart failure occurring. With this information, action could be taken prior to heart failure to minimize the response time of trained professionals. This type of continuous monitoring inherently calls for disposable, cost-efficient, real-time biosensors that are capable of very sensitive protein detection. *Chapter 2* illustrated that SWNTTFs were capable of real-time and ultrasensitive detection of viruses. With this in mind, the aim of this project is to fabricate a second platform for detection of human BNP using SWNTTF electrical biosensors on disposable PET substrates.

3.1 Fabrication and Methods

3.1.1 PET Device Fabrication and Characterization

The aim of this project was to realize a disposable chemiresistive SWNTTF device capable of detecting pg/mL concentrations of BNP. Therefore, to achieve a realistic disposable sensor system a cost-efficient substrate is a vital requirement. By customizing premade substrates that are conventionally used for blood glucose sensors, a cost effective proof-of-concept device can be fabricated. *Figure 3.2* shows the fully fabricated PET substrate for the SWNTTF based electrical biosensor.
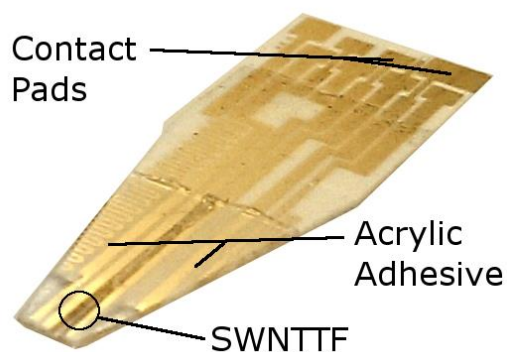
Figure 3.2: Image showing a PET based SWNTTF BNP test strip.

The device show in *figure 3.2* depicts how simple one of these SWNTTF based BNP test strips can be to fabricate. Three features on this device worth noting are the area where the SWNTTF is exposed, the pre-patterned gold electrodes and the acrylic adhesive. By removing the cover and cleaning the remaining adhesive layer, conventional glucose blood test strips are used as a substrate for SWNTTF chemiresistors. The SWNTTFs transferred to the PET substrate are akin to the SWNTTFs on the silicon based devices described in *section 2.2.1*. Two main differences from the silicon based growth and transfer include using a non-diluted catalyst for

growth and no PMMA coating to facilitate transfer. After bare SWNTTF transfer, an acrylic adhesive is used to passivate the gold electrodes so that only the SWNTTF and substrate beneath it are exposed to the various testing solutions. By doing this, interactions between the gold electrodes and the nanotubes are ruled out as a cause for an electrical response from the film. Fabrication and experimental set up for these devices can be seen in detail in *appendix A*.

Similar to the silicon based SWNTTF devices, it was very important to fully characterize these devices prior to testing. This is due to the fact that any unintended changes occurring during the synthesis or transfer could result in a test strip that is unusable. In light of this, dry state characterization, which can be seen in *figure 3.3*, was completed for each device.
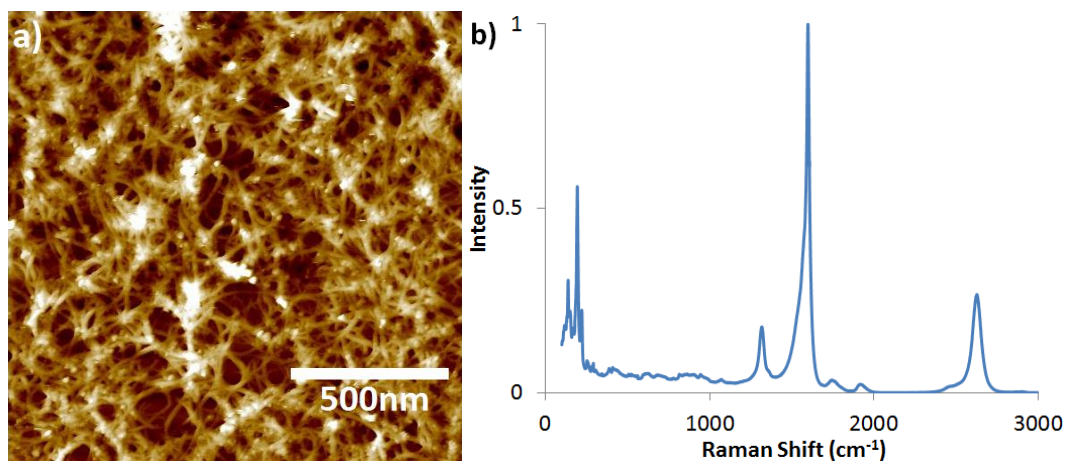
Figure 3.3: Dry state characterization of SWNTTF including (a) AFM image and (b) Raman spectroscopy.

Figure 3.3(a) shows that these films have a higher tube density than the films synthesized for the silicon based devices, meaning that a non-diluted catalyst was capable of promoting additional growth of SWNTs. The main purpose for using a higher density film was to facilitate a film transfer that does not require a PMMA coating. With higher density films the harsh DMSO cleaning protocol used for the silicon based devices can be avoided. The nanotube

diameter was not measureable for these films due to the fact that none could be imaged on a bare substrate because of the higher density. However, it is assumed that the majority of nanotubes are indeed single walled according to previous film characterization using the same protocol[86]. The Raman spectrum seen in *figure 3.3(b)* confirms SWNT growth using the non-diluted catalyst solution. The characteristic peaks of SWNTs (RBM, D band, G band and 2D band) discussed in *section 2.3.1* were all present in the samples used for testing.

3.2 Results and Discussion

3.2.1 pH Sensing

The first test completed on each SWNTTF device was the pH test. The reason this was done was in order to ensure that successful back end fabrication had occurred. Due to the difficult nature of passivating the electrodes by hand, it was observed that some films lost all exposed surface area and in turn became unusable. Further, pH testing was used to study the electrochemical effect it had on the higher density SWNTTFs on PET substrates. With this information, it is possible to see any response changes due to the substrate beneath the SWNTTF. All protocol pertaining to the device pH testing can be found in *appendix B*. Representative electrical responses to pH changes from a device can be found in *figure 3.4*.
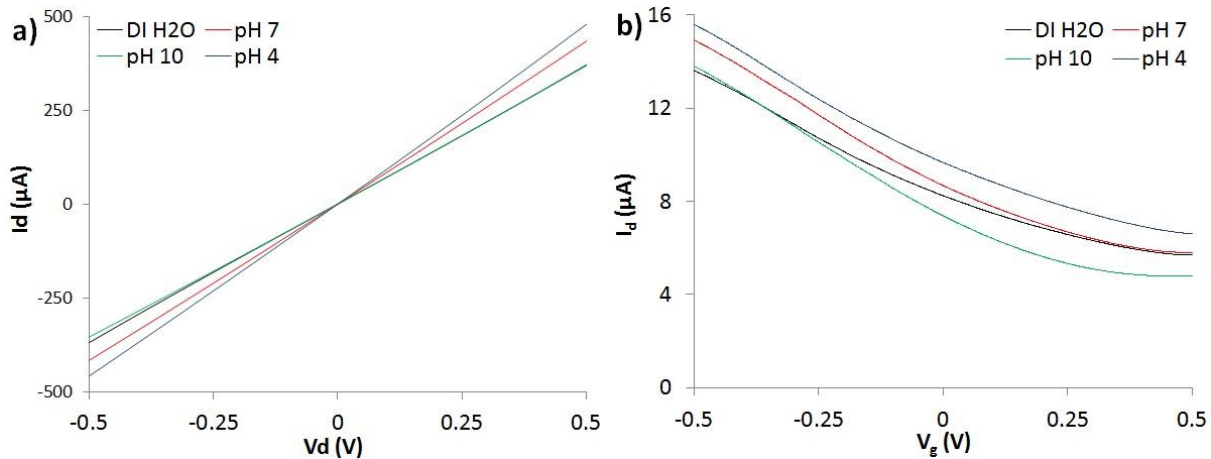
Figure 3.4: Representative PET based SWNTTF measurements taken during the pH test including (a) I_d-V_d and (b) I_d-V_g.

Figure 3.4(a) shows the I_d change corresponding to a changing V_d in DI H2O and 3 different 10mM phosphate buffers. A trend that was observed for all successful pH tests is an increasing resistance with increasing pH level, which was comparable to the silicon based SWNTTF response to pH changes. It is of note that the drain current of these devices showed a linear dependence on V_d, which was not observed in the silicon based devices.

Figure 3.4(b) shows the same film's response to pH using an I_d-V_g measurement. This is an additional test that was available for the PET based devices due to their unique setup. Analysis of the shape of the I_d-V_g response can lead to a number of conclusions. A similar trend to the I_d-V_d measurements can be seen in this case, where there is an increased I_d for the device when it is immersed in lower pH solutions. Further observation shows that switching to a lower pH solution seems to shift the whole curve upwards, meaning that a shift of the threshold voltage (V_{th}) is not the cause for I_d changes at different pH levels. This behaviour rules out electrostatic gating as the dominant mechanism[26]. Further, the slope of the subthreshold region (S_{th} = -5 V/dec for each curve) shows very little change between the three pH conditions, meaning that capacitive coupling is also not a dominant mechanism of sensing. With the

67

electrodes passivated, Schottky barrier modulation is also ruled out as no electrode/SWNT junction is exposed to solution. By process of elimination, these results show chemical doping or direct electron transfer between the H^+/OH^- ions and the SWNTTFF being the dominant sensing mechanism for these films. This corresponds well with the silicon based SWNTTF devices.

One interesting measurement to note is the SWNTTF's response to gating in DI H_2O. As the threshold voltage of the device does not seem to change, there is a clear subthreshold slope difference (S_{th} = -6.5 V/dec) in comparison to the measurements done in phosphate buffer. The cause of this is most likely due to a change to the capacitance seen in the double layer as additional ions are present in the buffered solution. With an increase to the double layer capacitance in buffered solutions, there will be a corresponding increase to the systems total capacitance, which in turn will increase the overall conductance of the film at a particular V_g. It is also worth noting that in all tests completed for these devices, the DI H_2O response to V_g changes seemed to be the most inconsistent in terms of the subthreshold slope.

3.2.2 BNP Detection

With all previous characterization completed, the SWNTTF test strips were then used to detect various concentrations of human BNP. The receptor molecules chosen for these experiments were a polyclonal anti-human BNP antibody (Phoenix Pharmaceuticals, Ltd.) and an anti-human BNP aptamer (OTC Biotech, Ltd.). These two different receptor molecules were chosen to determine if there was any sensitivity difference between the larger antibody and smaller aptamer. Theoretically, a smaller receptor should yield a higher sensitivity due to the

fact that it will ensure capture events occur closer to the surface of the transducer. The Debye length, discussed in detail in *section 1.3.1.1*, is an important factor that determines whether or not electrochemical events are screened from the surface of the transducer. This means that a smaller receptor molecule should theoretically give a larger response as capture events are more likely to happen within the Debye length.

A very important factor that must be taken into account when testing the BNP response of these test strips is their real-time response. The end goal of this project was to fabricate a device capable of monitoring an individual's BNP concentration in blood throughout the day. If the concentration of BNP in solution cannot be determined within minutes of the test being taken, the practicality of these devices is diminished. Protocol used to prepare each SWNTTF for the BNP detection test can be found in *appendix B*. *Figure 3.5* shows the real-time current response of two devices to a variety of human BNP (purchased from Sigma Aldrich, Co.) concentrations.
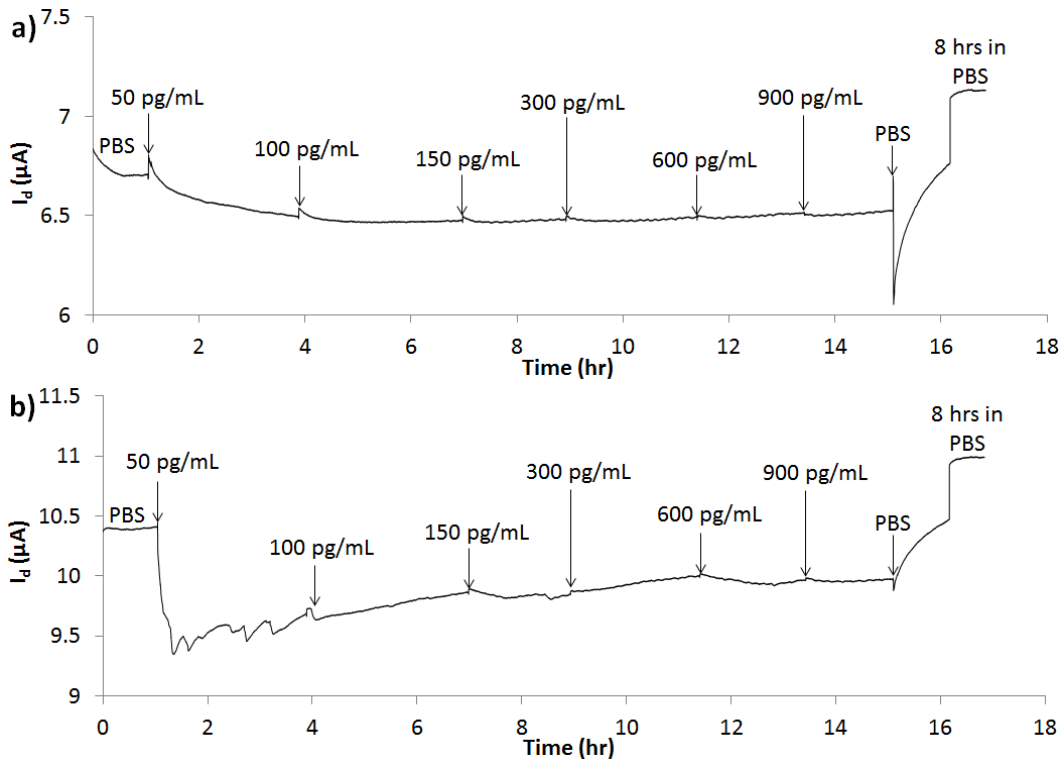
Figure 3.5: Real-time I_d response with respect to different BNP concentrations from an (a) aptamer coated SWNTTF and (b) antibody coated SWNTTF.

The graphs in *figure 3.5* show the preliminary results for real-time current responses from SWNTTF devices using aptamer (*figure 3.5(a)*) and antibody (*figure 3.5(b)*) as receptors at different BNP concentrations. The concentrations of BNP in 1x PBS used for these detection tests range from 50pg/mL to 900pg/mL, which correspond to below, within and above the "grey-zone" for BNP levels in blood described in *section 3.1*.

The first important observation that can be made from *figure 3.5* is the fact that both devices showed a significant response to BNP at 50pg/mL concentration. The PBS normalized resistance responses were $\Delta R/R_o$ = 3.54% and $\Delta R/R_o$ = 11.3% for the aptamer and antibody coated SWNTTFs, respectively. The signal change due to the addition of BNP is clearly above the electrical noise level meaning that successful detection of capture events did take place. The required time for aptamer coated device to have a stable current reading pertaining to a

70

normalized resistance change of 3.54% was approximately 2.5 hours. The antibody coated SWNTTF, however, did show a more immediate response to the BNP capture as the response time required to reach a normalized resistance change of 10.15% was 16 minutes.

Although these devices did show immediate sensitivity to the lower end of required detectable concentrations, the film behaviour subsequent to initial response must be analyzed. The aptamer coated device in *figure 3.5(a)* showed no response to the subsequent test concentrations, as the approximate normalized resistance of the film maintained a value of 3-3.5%. Despite the fact the antibody coated device in *figure 3.5(b)* showed a large initial increase in resistance, a stable current was never achieved. The device showed fluctuation as well as a gradual decrease in film resistance regardless of any additional BNP in solution. A PBS wash after all concentrations were introduced decreased the resistance of the film to a value close to the initial resistance before the test. Further, the drain current was seen to increase past the initial PBS drain current after an overnight soak.

No response from the aptamer coated device after the initial 50pg/mL could be a result of aptamer saturation. Further, the smaller normalized resistance change for these devices could be due to interactions between the pi network of the SWNTTF and the pi bonds within nucleobases. This may result in a deactivation of a percentage of aptamers for capture events, thereby decreasing the amount of electrical change of the device at all BNP concentrations. Fluctuation in current response from the antibody receptors could be caused by delamination of the antibody-BNP pair once a capture event occurs. The antibody device continually increased in drain current even with higher concentrations of BNP in solution. Interactions with

the BNP molecules seems to be the reason for this increase in drain current as the devices are quite stable in PBS prior to the BNP introduction.

3.3 Conclusions

Fabrication of cost-effective, disposable, real-time and sensitive SWNTTF chemiresistors on PET test strips is realized through this work. By testing the pH response of the films, sensing mechanisms discussed in the silicon based SWNTTF devices is confirmed. Preliminary results using aptamers and antibodies specific to BNP as the receptors demonstrate the successful detection of 50pg/mL concentration of human BNP in PBS. The aptamer coated test strip shows a normalized resistance increase of 3.5%, while the antibody coated test strip shows a normalized resistance increase of 11.3%. The electrical signal during these tests show either long required times to reach a stable signal (aptamer) or signal fluctuation throughout the test (antibody) occurred. Further experimentation is required to confirm these preliminary results.

3.4 Future Work

Reproducing the results seen in *section 3.2* is the first additional work that must be done for this project. This is due to the fact that the conclusions proposed must be confirmed before design changes are made to improve the system. With additional data and confirmation of the systems behaviour, an optimization of the test strip's design can take place. There are two observations made during experimentation that require immediate attention. These include the long signal stabilization time of the aptamer based test strips and the fluctuation of signal in the antibody based test strips.

Although there was a significant response from the devices to the lowest concentration of BNP, a few results are concerning. One issue that must be further studied is the stabilization of the electrical signal during detection experiments. The aptamer system requires incubation times of up to 3 hours before a stable signal is reached. Clearly, this is not favourable because these devices are meant to be real-time sensors so that the blood BNP levels can be monitored continuously throughout the day. Additional experimental data regarding the aptamer recognition of BNP and its induced signal in the SWNTTF is required. Further, study into the kinetics of diffusion and capture of BNP on SWNTTFs must be studied. With this information, a correlation between the kinetics of adsorption and the electrical response can be made. This correlation would then allow for extrapolation of the current *versus* time curve to determine the concentration of BNP in the blood within minutes.

The stabilization issues in the antibody system are of different a different nature. The current response of this system showed an immediate response (16 minutes) to BNP with signal fluctuation throughout the rest of the test. The antibody/BSA coated film was electrically stable in PBS prior to the addition of human BNP. This means that the interactions between the BNP molecules and the antibodies are causing the fluctuation in the current. As aforementioned, one potential cause for this that could be the antibody/BNP pair detaching from the surface after the molecule is captured from solution. Using another technique, such as a quartz crystal microbalance, future work could involve studying whether or not this detachment is the reason behind these current fluctuations. If detachment is the cause, work towards modifying the SWNTTF/recognition molecule through functionalization for potential carbodiimide chemistry would help to ensure that this detachment does not occur.

4. Summary

The main goal of this work is to demonstrate the capabilities of SWNTTF based chemiresistive biosensors. To achieve this, successful fabrication and characterization of two different platforms for biomolecule detection is required. The first allows for the study of effects that device geometry has on pH and M13 bacteriophage sensing capabilities as well as the underlying mechanisms governing SWNTTF chemiresistive biosensors. The second demonstrates the commercial potential of SWNTTF chemiresistive biosensors by detecting relevant concentrations of the BNP on economically viable substrates.

Successful detection of 0.5pM M13 bacteriophage was accomplished using 32 parallel SWNTTF chemiresistors on Si/SiO$_2$ substrates. The work demonstrated the real-time, sensitive and reproducible biosensing capabilities of these devices. Device design was used to vary SWNTTF geometry and dry state characteristics in order to study and isolate sensing mechanisms responsible for response to pH changes and M13 capture events. Chemical doping was determined to be the dominant sensing mechanism during pH tests for bare nanotubes, while other mechanisms became more significant as the SWNTs were coated with a layer of biomolecules. The mechanism responsible for resistance response to M13 capture events was determined to be electrostatic gating. However, device response did not exactly follow the expected trend for isolated electrostatic gating. Device geometry was observed to have an effect on the overall reproducibility and sensitivity of the device to capture events. Finally, a qualitative device calibration was accomplished in order to associate a resistance response to a specific concentration of M13.

Antibody saturation or excessive gating prior to M13 detection are potential reasons for the non-exponential resistance response of the SWNTTFs. Smaller increases to the concentration of M13 during detection tests as well as adsorption isotherms of M13 onto the films must be assessed. Gating during detection tests may also help to improve the sensitivity of the devices at this range of concentrations. Using this information a complete understanding of the electrical response to capture events can be achieved. By doing this, a quantitative approach to device calibration can be taken so that the response of a device to a single capture event can be determined. Further, modifications must be made to the device design as well as the receptor and SWNTTF in order to optimize sample delivery and film response.

A cost-efficient approach at fabricating SWNTTF chemiresistors on PET demonstrated devices capable of real-time and sensitive detection of relevant concentrations of human BNP. The pH resistance response of these devices confirm conclusions made in the Si/SiO$_2$ case as doping is the dominant sensing mechanism during pH tests. Preliminary results demonstrated significant resistance changes in the SWNTTF at BNP concentrations in PBS as low as 50pg/mL. Further, there was a noticeable difference in the magnitude of resistance change depending on the receptor molecule used to capture BNP.

This work requires more data in order to statistically verify results. Inconsistencies in preliminary results as well as current stability issues must also be addressed for the PET based devices. The aptamer coated SWNTTFs took a number of hours to stabilize while the antibody coated SWNTTFs exhibited fluctuations in current throughout tests. Determining the adsorption/desorption properties of BNP during capture events is vital to understanding the

nature of device response. Design considerations must be taken into account as detachment of biomolecules is a potential reason for these measurements. SWNTTF and receptor functionalization must be studied in order to address the stability issues. If extended periods of time are required for stabilization, additional data can allow for extrapolation and curve fitting in order to realize real-time detection.

This work has demonstrated that SWNTTFs as transducers in two different chemiresistive biosensors are capable of real-time, sensitive, selective and reproducible detection of biomolecules. This work not only gives insight into the sensing mechanisms governing SWNTTF based biosensors, it can also be consulted for device design considerations. With additional data regarding device design as well as SWNTTF density and geometry, optimal prototype properties can be determined in order to achieve a favourable sensitivity and reproducibility. This data provides additional information that aims to bridge the gap between research and commercialization of SWNTTF based electrical biosensors.

Appendix A – Fabrication

A.1 Silicon Based SWNTTF Devices

A.1.1 Single Walled Carbon Nanotube Thin Film Synthesis

The procedure for synthesizing SWNTTFs begins with the preparation of a catalyst solution. Firstly, 7nm silica nanoparticles are loaded with catalyst metals. This is done by dissolving 50mg of silica powder as well as 3.0mg of Iron (III) acetylacetonate, 0.7mg of Molybdenum (II) acetate and 4.6mg of Cobalt (II) acetate in two separate vials containing 10mL of ethanol. The solutions are then sonicated for 30 minutes and then mixed together. Once mixed, the solution is sonicated for an additional 2 hours. Sonication at this time promotes the impregnation of the catalyst metals into the pores of the silica nanoparticles. This is an important step as the duration of sonication determines the overall how well dispersed the nanoparticles are in solution which in turn controls the film's homogeneity. Once the catalyst is prepared, it can be diluted in order to control the density of the film. In order to get on currents (I_{on}) ranging in the few hundreds of nanoamps with I_{on}/I_{off} ranging from 2-3, the catalyst must be diluted by 10x in ethanol. An increase in the dilution from 10x to 30x will decrease the current while increasing the ratio of I_{on}/I_{off}. A complete study on the optical, mechanical and morphological characterization for these SWNTTFs has been previously reported[86].

Silicon/2μm SiO_2 (thermal) wafers are used as the growth substrates. Prior to coating the substrate with catalyst, the wafers are cleaned using RCA 1 protocol. This is done in order to remove any contaminants from the surface of the wafer and ensure that the SiO_2 surface is

hydroxylated[109]. The catalyst is able to completely and consistently wet the surface of the wafer when there are OH groups present. The diluted catalyst solution is then pipetted onto the surface of the wafer. The wafer is then spun at 2500rpm for 1 minute then immediately placed on a hot plate at 120°C for 5 minutes. Chemical vapour deposition is then used to grow the SWNTTF. The substrate is then placed into a 2 inch quartz tube CVD chamber in a high purity Argon (1200 sccm) and Hydrogen (36 sccm) environment. The temperature of the tube furnace is then ramped to the growth temperature of 850°C. Once the growth temperature is reached the flow of gas is diverted through an ethanol bubbler held at -1°C for 20 minutes. The bubbler is then bypassed and the chamber is allowed to cool to room temperature. A detailed study of the morphological, optical and electrical properties of these films has been reported[86].

A.1.2 Substrate Fabrication

Prior to any electrode deposition or patterning, the backside SiO_2 silicon wafers must be etched away in order to use the backside of the wafer as the gate electrode. First, the wafers are coated with 1.1μm of S1811 positive photoresist (Microchem) in order to protect the top side dielectric. The wafer is then placed in an ammonium fluoride buffered oxide etchant solution for 10 minutes. After the etching is complete, the wafer is washed in three different DI H_2O baths and finally blown dry with a nitrogen gun. The photoresist is then removed using sonication in acetone and finally blown dry with nitrogen. In order to ensure that there is no residual photoresist, the wafer is then oxygen plasma etched under 300mTorr and 1000W at 180°C for 120s in the CV200RFS oxygen plasma etching system (Yield Engineering Systems).

Electrodes for the devices are fabricated using conventional liftoff photolithography. Beginning with bare silicon/50nm SiO_2 (thermal) wafers, the wafers are coated with a monolayer of hexamethyldisilazane (HMDS) using the 310-TA (Yield Engineering Systems) HMDS coater in order to ensure that the substrate surface is hydrophobic for better adhesion to photoresists. A 1.1μm of layer of S1811 positive photoresist is then coated onto the wafer which is then soft baked at 115°C for 90 seconds. Using the photomask shown in *figure 2.1(b)*, the wafer is exposed to 120 mJ/cm^2 of UV light (365nm-405nm) using the MA-6 Aligner (Suss-Microtec). The wafer is then placed into a MF319 developer (Microchem) bath for approximately 45 seconds and is then rinsed with DI H_2O and placed in a DI H_2O bath for 5 minutes. Subsequent to patterning, the wafer is placed into nanochrome II e-beam evaporator (IntlVac) and coated with titanium/gold (5nm/50nm). Once removed from the chamber, the wafer is placed in acetone for 10 minutes. Harsh sonication in a new acetone bath helps to remove all residual gold from the wafer's surface. The wafer is then placed in an isopropanol bath followed by a DI H_2O bath and finally blown dry with nitrogen gas. In order to attain single substrates with 32 electrode pairs, the wafers are hand scribed into 1cm x 1cm chips.

A.1.3 SWNTTF Liftoff, Transfer, Patterning and Cleaning

In order to make use of the CVD grown SWNTTFs they must be transferred onto the electrode array. As the films are more than 95% transparent to the naked eye and extremely thin[86], they must first be coated with a 1.5μm poly(methyl methacrylate) (450A PMMA Microchem) film for mechanical and optical support. The PMMA is spin coated onto the growth substrate at 3500rpm for 60 seconds then placed on a hotplate at 60°C for 60 seconds. The film

is then hand etched into 2mm x 8mm rectangles that will be transferred onto the patterned electrodes. As the films are grown on and anchored onto a 2µm layer of SiO_2, a hydrofluoric acid bath is capable of wet etching the oxide layer to facilitate liftoff while leaving the PMMA/SWNT film unharmed[86]. The wafer is placed in a 5% HF in DI H_2O for approximately 20 seconds and swiftly placed into a 2L DI H_2O bath very slowly. The film is capable of free standing on the surface of the water due to its hydrophobic nature and the surface tension of water. Using a substrate that has been patterned with Ti/Au electrodes, the PMMA/SWNT film is lifted off the surface of the water and allowed to dry at room temperature to minimize wrinkling in the film.

Prior to patterning the film, the PMMA is gently removed by placing the substrate into a room temperature acetone bath overnight. The device is then rinsed with isopropanol and DI H_2O and blown dry with nitrogen. The SWNTTF is patterned into the four dimensions previously mentioned using photolithography coupled with dry etching. 1.1µm Shipley 1811 positive photoresist is spin coated onto the substrate containing the SWNTTF and then soft baked at 115°C for 90 seconds. The wafer is then exposed with approximately 120 mJ/cm^2 of UV light (365nm-405nm) through a photomask that exposes all areas of the substrate except the areas bridging the pairs of electrodes. This ensures that the unexposed areas of the film will be protected by a thick layer of photoresist for further processing. The substrates are then developed in MF319 developer (Microchem) bath for approximately 45 seconds and then rinsed with DI H_2O and placed in a DI H_2O bath for 5 minutes and finally blown dry with nitrogen. In order to burn away unwanted SWNTs and residual photoresist, the substrate was plasma etched at 20 mTorr and 100W oxygen plasma for 5 minutes.

The final device processing step before sensing experiments can be completed is cleaning the SWNTs of all residual photoresist and contaminants. This is arguably the most important step in fabrication because the overall sensitivity of the SWNTs during sensing is dictated by how much of the tube is actually exposed to its environment. Further, cleaning the substrate and SWNTTF was the step that yielded the most inconsistent results meaning further optimization of this protocol is required. Briefly, the substrate is place in a hot dimethyl sulphoxide (DMSO) bath at 170°C under agitation and covered by a watch glass. Being very close to the boiling point of DMSO it is very important that the temperature is closely monitored so that bubbling at the substrate surface does not occur. Any amount of bubbling has resulted in some of the films being torn from the substrate's surface. After 2 and 4 hours, the majority of the DMSO is pipetted out of the beaker and replaced with fresh DMSO that is allowed to ramp back up to 170°C. It is imperative that the substrates are not allowed to dry during the replacement of DMSO as this leads to residues and contaminants adhering very strongly to the surface of the substrate. After a total of 8 hours in the hot DMSO bath, the substrate is removed and placed into a room temperature DMSO/DI H_2O bath (1:1 volume) for 30 minutes. The substrate is then placed in a DI H_2O bath for 30 minutes and is finally blown dry with nitrogen.

A.1.4 PDMS Microfluidic Channel and Fluid Delivery

To fabricate the microfluidic channel, a negative mold composed of 3035 SU-8 (Microchem) was created on a silicon wafer. Wet PDMS (10:1 w/w of Polymer:Curing agent) was cured in the mold at 80°C for one hour and subsequently cut out of the mold. Inlet and

outlet holes for the fused silica (250µm inner diameter Polymicro Technologies) tubing were

drilled into the PDMS using a finger drill (#80 Micro-Mark). The microfluidic channel is then

aligned and placed onto the surface of the silicon device so that the SWNTTFs are exposed,

while all gold electrodes are passivated. *Figure A.1* shows the equipment used as well as the

final PDMS product used to create a microfluidic channel.
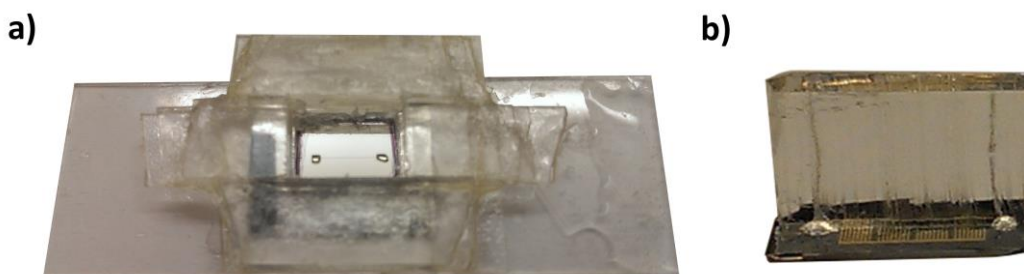
Figure A.1: Images concerning microfluidic channel fabrication including (a) PDMS master mold with reservoirs and microfluidic indent and (b) custom made PDMS slab with microfluidic channel and inlet/outlet holes.

The master PDMS mold and a fabricated PDMS slab, *figures A.1(a)* and *A.1(b)*,

respectively, are vital for device fabrication. Using this method of microfluidic sample transport,

a simple and robust way to deliver sample to the devices can be realized. Further this allows for

very small sample volumes which decreases the overall cost per test run. A Cheminert two-

position 10-port valve (Valco Instruments Co. Inc.) was used for sample switching during tests,

which can be seen in *figure A.2*.
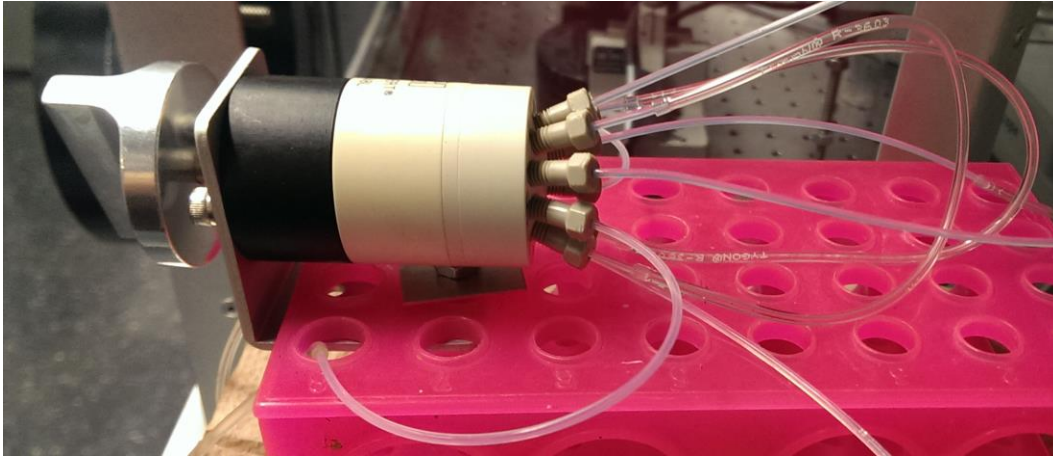
Figure A.2: Two position sample selector.

This device is capable of diverting flow through a second sample loop so that a direct switch from one sample to another can be achieved. This ensures that no additional washing steps occur between sample switching so that solution concentrations and pH levels are strictly controlled. Further, this setup does not require tubing removal which was seen to cause significant amount of noise during testing as well as device disconnection in some cases.

A.1.5 Custom Electrical Equipment

Due to the design requirements certain custom made parts and tools were necessary to fabricate a working prototype. As one of the main goals of this work was to realize multi-device sensing in parallel, incorporating a chip carrier into the final prototype was required. However, after exhaustive research into chip carriers it was realized that no conventional carrier and socket system was capable of meeting requirements regarding clamping PDMS onto the surface of the device or the liquid delivery system. In light of this, a chip carrier and socket system were designed and fabricated and can be seen in *figure A.2*.
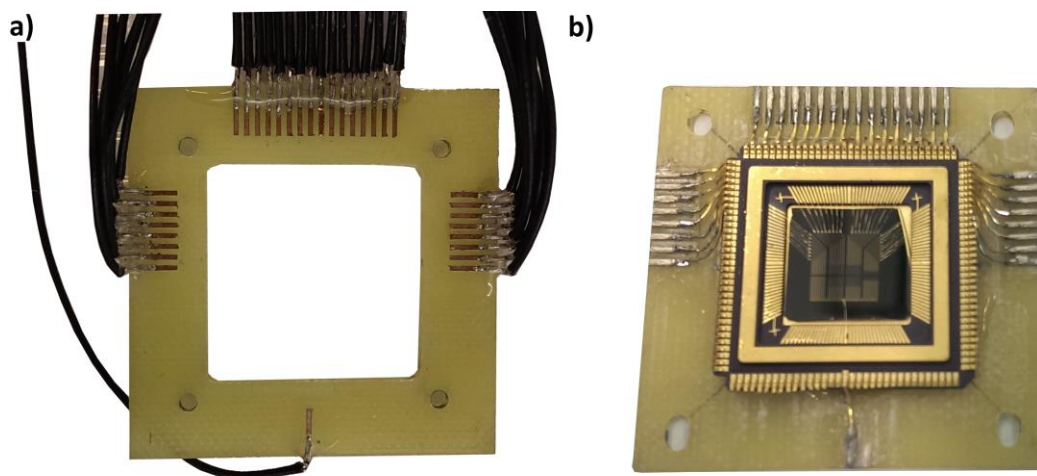
Figure A.3: Images of custom made (a) socket with electrical copper plating soldered to wires for probing and (b) chip carrier with leads soldered to socket and completely wire bonded to 32 electrode pairs.

Both prototype components seen in *figure A.3* were custom designed then milled from a non-conductive copper plated sheet. The design of the electrical socket can be seen in *figure A.3(a)*, where all 32 fingers lead to external wiring. The chip carrier (Spectrum Semiconductor Materials, Inc.) in *figure A.3(b)* was cut to fit the custom socket and subsequently soldered onto copper plating for alignment purposes. By using a gold wire bonder to connect the gold contact pads on the substrates to the external wires, artefacts and noise that result from using a probing station during experimentation were avoided. It was observed that any vibrations from movement to and from the probing station caused significant changes in the electrical reading of the device.

A.2 PET Based SWNTTF Devices

The fabrication of the PET based devices begins with preparing purchased glucose sensing test strips (Accuchek Aviva test strips, Hoffmann La Roche, Ltd.). *Figure A.4* shows the progression of the PET based test strips.
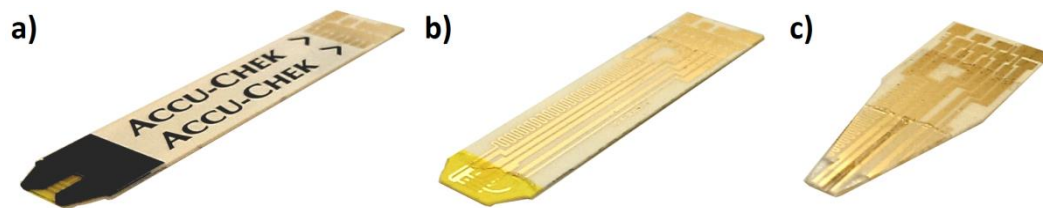
Figure A.4: Images concerning complete PET device fabrication including (a) purchased glucose meter test strip, (b) test strip with cover peeled off and (c) final device including a SWNTTF and acrylic adhesive.

Figure A.4 depicts the simple approach taken to realize a fully functional SWNTTF chemiresistor. Beginning with the purchased test strip *figure A.4(a)*, simply peeling the top cover off of the test strip gives access to the patterned gold electrodes and glucose-oxidase coated region seen in *figure A.4(b)*. The area used for glucose sensing is then cut off and left over adhesive is then removed by rubbing the electrodes in an acetone bath. A patterned SWNTTF is then transferred into the region between two adjacent electrodes. Transfer of the SWNTTF is akin to transfer techniques described in *section 2.2.3* with no PMMA support required for these higher density films. Electrodes are then passivated by aligning an acrylic adhesive (McMaster Carr, Ltd), which can be seen as the final test strip prototype in *figure A.4(c)*.

Appendix B – Test Protocol

A.1 Silicon Based SWNTTF Devices

Prior to any pH or biomolecule detection tests, to ensure that leakage within the device is not occurring water was used for a seal check. Typical tests involved using a peristaltic pump to deliver a variety of solutions through the microfluidic channel of the device. During experimentation, it was observed that the additional pressure increase that occurs periodically with peristaltic pumps introduces a periodic increase in electrical signal from the devices. Due to this pressure increase, pump was run for 30 minutes in order to ensure that the sample solution was indeed in the microfluidic channel and subsequently turned off. Once turned off the signal was allowed to stabilize prior to taking any resistance measurements. The signal stabilization typically took 5-10 minutes after the pump was turned off.

The pH test was the first test completed on the devices once they were mounted into the final prototype. Protocol for this test involved using three different phosphate buffered solutions after a stable signal was achieved in DI H_2O. The solutions were all made at 10mM in Milli-Q H_2O with pH levels of pH 10, pH 7 and pH 4. The devices were exposed to each pH level for 30 minutes with pumping and an additional 10 minutes after the pump was stopped.

Subsequent to pH testing, the M13 detection tests were run on the devices beginning with introducing 1x phosphate buffered saline (PBS) into the microfluidic channel. Once a stable signal is achieved, the baseline resistance (R_{PBS1}) measurements are taken for all channels. After this, the SWNTTFs are decorated with receptor molecules specific to the target analyte. This is done first to ensure that the receptor molecules do not have to compete for a spot on the

device's surface and are free to physisorb onto any part of the substrate or SWNTTF. As the receptor adsorption is somewhat uncontrolled, it is ideal to introduce a copious amount of receptor molecules into the microfluidic channel. This study involved using an approximately 150kDa monoclonal anti-M13 pIII antibody (New England Biolabs Ltd.) in order to recognize and capture the pIII coat protein of the M13 bacteriophage. By incubating the SWNTTFs in 100nM M13 Ab in 1x PBS a significant electrical signal was detected in the devices indicating enough interaction occurred between the SWNTs and the M13 Ab. At this time, the resistance of the film (R_{M13Ab}) is measured for all channels. Non-specific binding must be ruled as a reason for electrically detecting a biomolecule, meaning that there must be no direct interactions between a target analyte and a bare SWNT. This leads to the next step where 1% Bovine serum albumin (BSA) in PBS (1mg BSA in 1mL PBS) is used to block off all remaining areas of the devices that were not coated with M13 Ab molecules. At this point, film resistance (R_{BSA}) is measured. A second 1x PBS wash is then completed to ensure that the microfluidic channel is depleted of all biomolecules. Once a stable signal is reached the film resistance (R_{PBS2}) is measured. Finally, the M13 detection test can begin by sequentially introducing three different M13 bacteriophage concentrations into the microfluidic channel. The three concentrations in order used in this study are 0.5pM, 5pM and 50pM of M13 in 1x PBS and in each solution the film resistance is measured as $R_{0.5pM\ M13}$, $R_{5pM\ M13}$ and $R_{50pM\ M13}$, respectively.

B.2 PET Based SWNTTF Devices

In order to electrically probe the devices during experimentation, a custom setup was required. As only a portion of the electrodes were passivated by the acrylic coating, dipping the

test strip into the test solution was required so that only the SWNTTF bridging the gold electrodes would be exposed to the sample. *Figure B.1* shows the experimental setup used to this end.
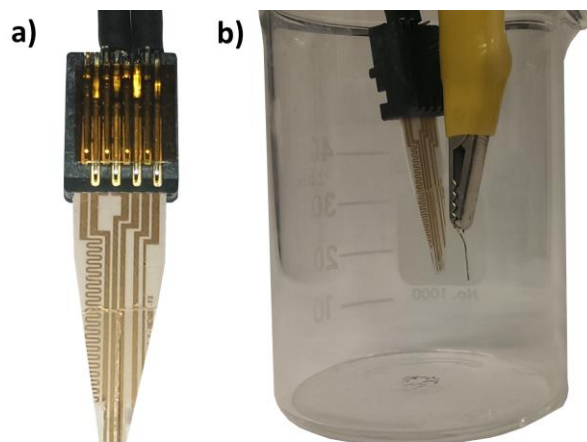
Figure B.1: Image of PET based SWNTTF device (a) slotted into customized test strip socket and (b) during a dip test with the platinum gate probe.

In order to fabricate the dip based socket for our testing seen in *figure B.1(a)*, the Accuchek Aviva glucose blood meter was disassembled. The socket used to electrically monitor the test strips for these sensors was then removed and soldered to triaxial cables in order to electrically probe the dip based system with the semiconductor analyzer. *Figure B.1.(b)* shows how the typical dip based test was run by immersing the end of the test strip and the platinum gate probe into solution.

In order to test the films response to pH, the device was first allowed to soak overnight in DI H_2O. After this, the SWNTTF area was dipped into a 10mM pH 10 phosphate buffer for 30 minutes. At this point the I_d-V_d measurement was taken varying V_d from -0.5V to 0.5V and the I_d-V_g measurement was taken varying V_g from -0.5V to 0.5V. The sample was then dipped into

pH 7 buffer for 30 minutes and pH 4 buffer for 30 minutes where the same measurements were taken in each condition.

BNP sensing involved soaking the electrodes in PBS overnight subsequent to the pH test. After the PBS soak, the devices were soaked in a 100nM solution of anti-BNP 3 aptamer (OTC Biotech, Ltd.) or polyclonal anti-human BNP antibody (Phoenix Pharmaceuticals, Ltd.) for approximately 8 hours. The antibody/aptamer solution was then replaced with a 1% (w/v) solution of BSA in PBS overnight. The devices were then rinsed in fresh 1x PBS overnight. At this point an I_d-V_d measurement is taken. With the V_d set to 10mV, the current is monitored as test strip is immersed into various concentrations of human BNP. The levels of the test BNP concentrations are: 50pg/mL, 100pg/mL, 150pg/mL, 300pg/mL, 600pg/mL and finally 900pg/mL. The current is monitored throughout the test and the current is allowed to stabilize before the solution is switched to the next concentration. After the test the electrode is placed back in PBS for another I_d-V_d measurement.

References

1.	Veetil, J. V & Ye, K. Development of Immunosensors Using Carbon Nanotubes. *Biotechnol. Prog.* **23,** 517–531 (2007).

2.	Dantham, V. R. *et al.* Label-Free Detection of Single Protein Using a Nanoplasmonic-Photonic Hybrid Microcavity. *Nano Lett.* **13,** 3347–3351 (2013).

3.	He, L., Ozdemir, S. K., Zhu, J., Kim, W. & Yang, L. Detecting single viruses and nanoparticles using whispering gallery microlasers. *Nat. Nanotechnol.* **6,** 428–32 (2011).

4.	Vollmer, F., Arnold, S. & Keng, D. Single virus detection from the reactive shift of a whispering-gallery mode. *Proc. Natl. Acad. Sci. U. S. A.* **105,** 20701–20704 (2008).

5.	Washburn, A. L., Luchansky, M. S., Bowman, A. L. & Bailey, R. C. Quantitative , Label-Free Detection of Five Protein Biomarkers Using Multiplexed Arrays of Silicon Photonic Microring Resonators. *Anal. Chem.* **82,** 69–72 (2010).

6.	Zhu, H., White, I. M., Suter, J. D., Zourob, M. & Fan, X. Opto-fluidic micro-ring resonator for sensitive label-free viral detection. *Analyst* **133,** 356–360 (2008).

7.	Huang, M. J. *et al.* Serotype-Specific Identification of Dengue Virus by Silicon Nanowire Array Biosensor. *J. Nanosci. Nanotechnol.* **13,** 3810–3817 (2013).

8.	Huang, Y.-W. *et al.* Real-Time and Label-Free Detection of the Prostate-Specific Antigen in Human Serum by a Polycrystalline Silicon Nanowire Field-Effect Transistor Biosensor. *Anal. Chem.* **85,** 7912–7918 (2013).

9.	Patolsky, F. *et al.* Electrical detection of single viruses. *Proc. Natl. Acad. Sci. U. S. A.* **101,** 14017–22 (2004).

10.	Shirale, D. J. *et al.* Label-free chemiresistive immunosensors for viruses. *Environ. Sci. Technol.* **44,** 9030–5 (2010).

11.	Tuan, C. Van, Huy, T. Q., Hieu, N. Van, Tuan, M. A. & Trung, T. Polyaniline Nanowires-Based Electrochemical Immunosensor for Label Free Detection of Japanese Encephalitis Virus. *Anal. Lett.* **46,** 1229–1240 (2013).

12.	Vidic, J. *et al.* Surface Plasmon Resonance Immunosensor for Detection of PB1-F2 Influenza A Virus Protein in Infected Biological Samples. *J. Anal. Bioanal. Tech.* **S7,** 1–7 (2013).

13.	Wang, S. *et al.* Label-free imaging, detection, and mass measurement of single viruses by surface plasmon resonance. *Proc. Natl. Acad. Sci. U. S. A.* **107,** 16028–32 (2010).

14. Yakes, B. J. *et al.* Surface plasmon resonance biosensor for detection of feline calicivirus, a surrogate for norovirus. *Int. J. Food Microbiol.* **162,** 152–158 (2013).

15. Zeng, C. *et al.* Rapid and sensitive detection of maize chlorotic mottle virus using surface plasmon resonance-based biosensor. *Anal. Biochem.* **440,** 18–22 (2013).

16. Bergveld, P. Development of an ion-sensitive solid-state device for neurophysiologial measurements. *IEEE Trans. Biomed. Eng.* **BME-17,** 70–71 (1970).

17. Nair, P. R. & Alam, M. A. Performance limits of nanobiosensors. *Appl. Phys. Lett.* **88,** 233120 (2006).

18. Luo, X. & Davis, J. J. Electrical biosensors and the label free detection of protein disease biomarkers. *Chem. Soc. Rev.* **42,** 5944–62 (2013).

19. Feigel, I. M., Vedala, H. & Star, A. Biosensors based on one-dimensional nanostructures. *J. Mater. Chem.* **21,** 8940–8954 (2011).

20. Mandal, H. S., Su, Z., Ward, A. & Tang, X. Carbon nanotube thin film biosensors for sensitive and reproducible whole virus detection. *Theranostics* **2,** 251–257 (2012).

21. Zhang, G.-J. & Ning, Y. Silicon nanowire biosensor and its applications in disease diagnostics: a review. *Anal. Chim. Acta* **749,** 1–15 (2012).

22. Nair, P. R. & Alam, M. A. Screening-limited response of nanobiosensors. *Nano Lett.* **8,** 1281–1285 (2008).

23. Nair, P. R. & Alam, M. A. Theory of "Selectivity" of label-free nanobiosensors: A geometro-physical perspective. *J. Appl. Phys.* **107,** 64701 (2010).

24. Nair, P. R. & Alam, M. A. Dimensionally Frustrated Diffusion towards Fractal Adsorbers. *Phys. Rev. Lett.* **99,** 256101 (2007).

25. Lee, K., Nair, P. R., Scott, A., Alam, M. a. & Janes, D. B. Device considerations for development of conductance-based biosensors. *J. Appl. Phys.* **105,** 102046 (2009).

26. Heller, I. *et al.* Identifying the Mechanism of Biosensing with Carbon Nanotube Transistors. *Nano Lett.* **8,** 591–595 (2008).

27. Kong, J. *et al.* Nanotube Molecular Wires as Chemical Sensors. *Science (80-.).* **287,** 622–625 (2000).

28. Besteman, K., Lee, J., Wiertz, F. G. M., Heering, H. A. & Dekker, C. Enzyme-Coated Carbon Nanotubes as Single-Molecule Biosensors. *Nano Lett.* **3,** 727–730 (2003).

29. Boussaad, S. *et al.* In situ detection of cytochrome c adsorption with single walled carbon nanotube device. *Chem. Commun.* 1502–1503 (2003).

30. Kocabas, C., Shim, M. & Rogers, J. A. Spatially Selective Guided Growth of High-Coverage Arrays and Random Networks of Single-Walled Carbon Nanotubes and Their Integration into Electronic Devices. *J. Am. Chem. Soc.* **128,** 4540–4541 (2006).

31. Snow, E. S. & Perkins, F. K. Capacitance and Conductance of Single-Walled Carbon Nanotubes in the Presence of Chemical Vapors. *Nano Lett.* **5,** 2414–2417 (2005).

32. Ishikawa, F. N. *et al.* Importance of controlling nanotube density for highly sensitive and reliable biosensors functional in physiological conditions. *ACS Nano* **4,** 6914–6922 (2010).

33. Salehi-khojin, A. *et al.* On the Sensing Mechanism in Carbon Nanotube Chemiresistors. *ACS Nano* **5,** 153–158 (2011).

34. Liu, Y., Li, X., Dokmeci, M. R. & Wang, M. L. Carbon Nanotube Sensors Integrated Inside a Microfluidic Channel for Water Quality Monitoring. *Sensors Smart Struct. Technol. Civil, Mech. Aerosp. Syst.* **7981,** 1–8 (2011).

35. Tey, J. N., Wijaya, I. P. M., Wang, Z., Goh, W. H. & Palaniappan, A. Laminated , microfluidic-integrated carbon nanotube based biosensors. *Appl. Phys. Lett.* **94,** 013107 (2009).

36. Lee, D., Chander, Y., Goyal, S. M. & Cui, T. Carbon nanotube electric immunoassay for the detection of swine influenza virus H1N1. *Biosens. Bioelectron.* **26,** 3482–7 (2011).

37. Jacobs, C. B., Peairs, M. J. & Venton, B. J. Review: Carbon nanotube based electrochemical sensors for biomolecules. *Anal. Chim. Acta* **662,** 105–127 (2010).

38. Li, W.-S. *et al.* High-quality, highly concentrated semiconducting single-wall carbon nanotubes for use in field effect transistors and biosensors. *ACS Nano* **7,** 6831–6839 (2013).

39. Malhotra, R., Patel, V., Vaque, J. P., Gutkind, J. S. & Rusling, J. F. Ultrasensitive Electrochemical Immunosensor for Oral Cancer Biomarker IL-6 Using Carbon Nanotube Forest Electrodes and Multilabel Amplification. *Anal. Chem.* **82,** 3118–3123 (2010).

40. Dong, B. X. *et al.* Electrical Detection of Femtomolar DNA via Gold-Nanoparticle Enhancement in Carbon-Nanotube-Network Field-Effect Transistors. *Adv. Mater.* **20,** 2389–2393 (2008).

41. Odom, T. W., Huang, J., Kim, P. & Lieber, C. M. Atomic structure and electronic properties of single-walled carbon nanotubes. *Nature* **391,** 62–64 (1998).

42. Grüner, G. Carbon nanotube transistors for biosensing applications. *Anal. Bioanal. Chem.* **384,** 322–335 (2006).

43. Saito, R., Fujita, M., Dresselhaus, G. & Dresselhaus, M. S. Electronic structure of chiral graphene tubules structure of chiral graphene tubules. *Appl. Phys. Lett.* **60,** 2204–2206 (1992).

44. Minot, E. D. Tuning the band structure of carbon nanotubes. *Cornell Univ.* **PhD Thesis,** 1–132 (2004).

45.   Charlier, J. Electronic and transport properties of nanotubes. *Rev. Mod. Phys.* **79,** 677–732 (2007).

46.   Fam, D. W. H., Palaniappan, A., Tok, a. I. Y., Liedberg, B. & Moochhala, S. M. A review on technological aspects influencing commercialization of carbon nanotube sensors. *Sensors Actuators B Chem.* **157,** 1–7 (2011).

47.   Martel, R., Schmidt, T., Shea, H. R., Hertel, T. & Avouris, P. Single- and multi-wall carbon nanotube field-effect transistors. *Appl. Phys. Lett.* **73,** 2447–2449 (1998).

48.   Tans, S. J., Verschueren, A. R. M. & Dekker, C. Room-temperature transistor based on a single carbon nanotube. *Nature* **393,** 49–52 (1998).

49.   Larrimore, L., Nad, S., Zhou, X., Abruña, H. & McEuen, P. L. Probing electrostatic potentials in solution with carbon nanotube transistors. *Nano Lett.* **6,** 1329–1333 (2006).

50.   Star, A., Gabriel, J. P., Bradley, K. & Grüner, G. Electronic Detection of Specific Protein Binding Using Nanotube FET Devices. *Nano Lett.* **3,** 459–463 (2003).

51.   Bradley, K., Gabriel, J.-C., Briman, M., Star, A. & Grüner, G. Charge Transfer from Ammonia Physisorbed on Nanotubes. *Phys. Rev. Lett.* **91,** 218301 (2003).

52.   Bradley, K., Briman, M., Star, A. & Grüner, G. Charge Transfer from Adsorbed Proteins. *Nano Lett.* **4,** 253–256 (2004).

53.   Takeda, S. *et al.* A pH sensor based on electric properties of nanotubes on a glass substrate. *Nanoscale Res. Lett.* 207–212 (2007).

54.   Liu, X. *et al.* Band engineering of carbon nanotube field-effect transistors via selected area chemical gating. *Appl. Phys. Lett.* **86,** 243501 (2005).

55.   Chen, R. J. *et al.* Noncovalent functionalization of carbon nanotubes for highly specific electronic biosensors. *Proc. Natl. Acad. Sci. U. S. A.* **100,** 4984–4989 (2003).

56.   Leyden, M. R. *et al.* Fabrication and Characterization of Carbon Nanotube Field-Effect Transistor Biosensors. *Proc. SPIE 7779, Org. Semicond. Sensors Bioelectron. III* **7779,** 77790H (2010).

57.   Artyukhin, A. B. *et al.* Controlled Electrostatic Gating of Carbon Nanotube FET Devices. *Nano Lett.* **6,** 2080–2085 (2006).

58.   Byon, H. R. & Choi, H. C. Network single-walled carbon nanotube-field effect transistors (SWNT-FETs) with increased Schottky contact area for highly sensitive biosensor applications. *J. Am. Chem. Soc.* **128,** 2188–2189 (2006).

59.   Tang, X., Bansaruntip, S., Nakayama, N. & Yenilmez, E. Carbon Nanotube DNA Sensor and Sensing Mechanism. *Nano Lett.* **6,** 1632–1636 (2006).

60.   Javey, A., Guo, J., Wang, Q., Lundstrom, M. & Dai, H. Ballistic carbon nanotube field-effect transistors. *Nature* **424,** 654–657 (2003).

61.   Chen, R. J. *et al.* An Investigation of the Mechanisms of Electronic Sensing of Protein Adsorption on Carbon Nanotube Devices. *J. Am. Chem. Soc.* **5,** 1563–1568 (2004).

62.   Hur, S.-H. *et al.* Organic nanodielectrics for low voltage carbon nanotube thin film transistors and complementary logic gates. *J. Am. Chem. Soc.* **127,** 13808–13809 (2005).

63.   Rosenblatt, S. *et al.* High Performance Electrolyte Gated Carbon Nanotube Transistors. *Nano Lett.* **2,** 869–872 (2002).

64.   Cao, Q. *et al.* Gate capacitance coupling of singled-walled carbon nanotube thin-film transistors. *Appl. Phys. Lett.* **90,** 023516 (2007).

65.   Maroto, A. & Balasubramanian, K. Functionalized Metallic Carbon Nanotube Devices for pH Sensing. *ChemPhysChem* **8,** 220 – 223 (2007).

66.   Hecht, D. S. *et al.* Bioinspired Detection of Light Using a Nanotube Field Effect Transistor. *Nano Lett.* **6,** 2031–2036 (2006).

67.   Salgin, S., Salgin, U. & Bahadir, S. Zeta Potentials and Isoelectric Points of Biomolecules: The Effects of Ion Types and Ionic Strengths. *Int. J. Electrochem. Sci.* **7,** 12404–12414 (2012).

68.   Schoning, M. & Poghossian, A. Recent advances in biologically sensitive field-effect transistors (BioFETs). *Analyst* **127,** 1137–1151 (2002).

69.   Davis, J. A., Jamest, R. O. & Leckie, J. O. Surface Ionization and Complexation at the Oxide/Water Interface. *J. Colloid Interface Sci.* **63,** 480–499 (1978).

70.   Zahab, A., Spina, L., Poncharal, P. & Marliere, C. Water-vapor effect on the electrical conductivity of a single-walled carbon nanotube mat. *Phys. Rev. B* **62,** 0–3 (2000).

71.   Tersoff, J. Schottky barrier heights and the continuum of gap sites. *Phys. Rev. Lett.* **52,** 465–468 (1984).

72.   Léonard, F. & Tersoff, J. Role of Fermi-Level Pinning in Nanotube Schottky Diodes. *Phys. Rev. Lett.* **84,** 4693–4696 (2000).

73.   Chen, R. J. *et al.* An Investigation of the Mechanisms of Electronic Sensing of Protein Adsorption on Carbon Nanotube Devices. *J. Am. Chem. Soc.* 1563–1568 (2004).

74.   Topinka, M. A. *et al.* Charge Transport in Interpenetrating Networks of Semiconducting and Metallic Carbon Nanotubes. *Nano Lett.* **9,** 1866–1871 (2009).

75.   Heller, I., Kong, J., Williams, K. A., Dekker, C. & Lemay, S. G. Electrochemistry at Single-Walled Carbon Nanotubes : The Role of Band Structure and Quantum Capacitance. *J. Am. Chem. Soc.* **128,** 7353–7359 (2006).

76.   Lohse, J., Dahl, O. & Nielsen, P. E. Double duplex invasion by peptide nucleic acid : A general principle for sequence-specific targeting of double-stranded DNA. *Proc. Natl. Acad. Sci. U. S. A.* **96,** 11804–11808 (1999).

77.   Young, M. E., Carroad, P. A. & Bell, R. L. Estimation of Diffusion Coefficients of Proteins. *Biotechnol. Bioeng.* **22,** 947–955 (1980).

78.   Jakes, K. S., Davis, N. G. & Zinder, N. D. A Hybrid Toxin from Bacteriophage fl Attachment Protein and Colicin E3 Has Altered Cell Receptor Specificity. *J. Bacteriol.* **170,** 4231–4238 (1988).

79.   Stengele, I., Bross, P., Garccs, X., Giray, J. & Wasched, I. Dissection of function domains in phage fd adsorption protein. *J. Mol. Biol.* **212,** 143–149 (1990).

80.   Newman, J., Swinney, H. L. & Day, L. A. Hydrodynamic properties and structure of fd virus. *J. Mol. Biol.* **116,** 593–603 (1977).

81.   Sidhu, S. S. Engineering M13 for phage display. *Biomol. Eng.* **18,** 57–63 (2001).

82.   Minot, E. D. *et al.* Carbon nanotube biosensors: The critical role of the reference electrode. *Applied* **91,** 093507–1–3 (2007).

83.   Jorio, A. *et al.* Characterizing carbon nanotube samples with resonance Raman scattering. *New J. Phys.* **139,** 1–17 (2003).

84.   Hu, L., Hecht, D. S. & Gruner, G. Percolation in Transparent and Conducting Carbon Nanotube Networks. *Nano Lett.* **4,** 2513–2517 (2004).

85.   Salvetat, J.-P. *et al.* Elastic and Shear Moduli of Single-Walled Carbon Nanotube Ropes. *Phys. Rev. Lett.* **82,** 944–947 (1999).

86.   Mandal, H. S., Ward, A. & Tang, X. Transferable thin films of pristine carbon nanotubes. *J. Nanosci. Nanotechnol.* **11,** 3265–3272 (2011).

87.   Kocabas, C. *et al.* Experimental and theoretical studies of transport through large scale, partially aligned arrays of single-walled carbon nanotubes in thin film type transistors. *Nano Lett.* **7,** 1195–1202 (2007).

88.   Back, J. H. & Shim, M. pH-dependent electron-transport properties of carbon nanotubes. *Jounal Phys. Chem. B* **110,** 23736–23741 (2006).

89.   Haeberle, T. *et al.* Solution processable carbon nanotube network thin-film transistors operated in electrolytic solutions at various pH. *Appl. Phys. Lett.* **101,** 223101 (2012).

90. Heller, I. *et al.* Influence of electrolyte composition on liquid-gated carbon nanotube and graphene transistors. *J. Am. Chem. Soc.* **132,** 17149–17156 (2010).

91. Munzer, A. M. *et al.* Back-gated spray-deposited carbon nanotube thin film transistors operatrd in electrolytic solutions: an assessment towards future biosensing applications. *J. Mater. Chem. B* **1,** 3797–3802 (2013).

92. Li, P., Martin, C. M., Yeung, K. K. & Xue, W. Dielectrophoresis aligned single-walled carbon nanotubes as pH sensors. *Biosensors* **1,** 23–35 (2011).

93. Lee, D., Cui, T. & Member, S. Layer-by-Layer Self-Assembled Single-Walled Carbon Nanotubes Based Ion-Sensitive Conductometric Glucose Biosensors. *IEEE Sens. J.* **9,** 449–456 (2009).

94. Chien, Y.-S. *et al.* The pH Sensing Characteristics of the Extended-Gate Field-Effect Transistors of Multi-Walled Carbon-Nanotube Thin Film Using Low-Temperature Ultrasonic Spray Method. *J. Nanosci. Nanotechnol.* **12,** 5423–5428 (2012).

95. Wu, Z. *et al.* Transparent , Conductive Carbon Nanotube Films. *Science (80-.).* **305,** 1273–1276 (2004).

96. Pati, R., Zhang, Y., Nayak, S. K. & Ajayan, P. M. Effect of H2O adsorption on electron transport in a carbon nanotube. *Appl. Phys. Lett.* **81,** 2638–2640 (2002).

97. Iler, R. K. *Chemistry of Silica: Solubility, Polymerization, Colloid and Surface Properties and Biochemistry of Silica*. 896 (Wiley - Interscience, 1979).

98. Yao, Z., Postma, H. W. C., Balents, L. & Dekker, C. Carbon nanotube intramolecular junctions. *Nature* **402,** 273–276 (1999).

99. Fuhrer, M. S. *et al.* Crossed Nanotube Junctions. *Science (80-.).* **288,** 494–497 (2000).

100. Kojio, K., Takahara, A. & Kajiyama, T. Bovine serum albumin adsorption onto immobilized organotrichlorosilane surface: Influence of the phase separation on protein adsorption patterns. *J. Biomater. Sci. Polym. Ed.* **9,** 131–150 (1998).

101. Peng, Z. G., Hidajat, K. & Uddin, M. S. Adsorption of bovine serum albumin on nanosized magnetic particles. *J. Colloid Interface Sci.* **271,** 277–283 (2004).

102. Lee, W.-K., Ko, J.-S. & Kim, H.-M. Effect of electrostatic interaction on the adsorption of globular proteins on octacalcium phosphate crystal film. *J. Colloid Interface Sci.* **246,** 70–7 (2002).

103. Chun, K. & Stroeve, P. Protein Transport in Nanoporous Membranes Modified with Self-Assembled Monolayers of Functionalized Thiols. *Langmuir* **18,** 4653–4658 (2002).

104. Morrison, L. K. *et al.* Utility of a rapid B-natriuretic peptide assay in differentiating congestive heart failure from lung disease in patients presenting with dyspnea. *J. Am. Coll. Cardiol.* **39,** 202–209 (2002).

105.   Maisel, A. *et al.* Rapid measurement of b-type natriuretic peptide in the emergency diagnosis of heart failure. *N. Engl. J. Med.* **347,** 161–167 (2002).

106.   Hall, C. Essential biochemistry and physiology of (NT-pro)BNP. *Eur. J. Heart Fail.* **6,** 257–260 (2004).

107.   Brenden, C. K. *et al.* Gray zone BNP levels in heart failure patients in the emergency department : Results from the Rapid Emergency Department Heart Failure Outpatient Trial (REDHOT) multicenter study. *Am. Heart J.* **151,** 1006–1011 (2006).

108.   Chin, C. D., Linder, V. & Sia, S. K. Commercialization of microfluidic point-of-care diagnostic devices. *Lab Chip* **12,** 2118–34 (2012).

109.   Burkman, D. C., Deal, D., Grant, D. & Peterson, C. A. in *Handb. Semicond. wafer Clean. Technol.* (Kern, W.) 111–151 (Boyes Publications, 1993).